Results in Engineering 31 (2026) 111420

Contents lists available at ScienceDirect

Results in Engineering

journal homepage: www.sciencedirect.com/journal/results-in-engineering

Research paper

Comparative analysis of optimization techniques for sizing and location of distributed generation in grid-connected microgrid

Kayode Ebenezer Ojo [a], Akshay Kumar Saha [a,*], Viranjay M. Srivastava [a,b]

[a] Discipline of Electrical, Electronic and Computer Engineering, University of KwaZulu-Natal, Durban 4041, South Africa
[b] Department of Electronics Engineering, Birmingham City University, Birmingham B4 7XG, UK

ARTICLE INFO

Keywords:
Active power loss
Bat algorithm
Distributed generation
Loss reduction
Particle swarm optimization
Quantum PSO
Sizing and location
Voltage magnitude

ABSTRACT

Efficient Distributed Generation (DG) sizing and allocation require advanced optimization techniques that facilitate real-time decision-making, improve power quality, reduce losses, and boost system performance while retaining cost efficiency. When searching in excessively complicated search spaces without parameter fine-tuning, conventional evolutionary optimization approaches frequently fail to identify global optima and become trapped in local optima. This research proposes three different optimization techniques, including Particle Swarm Optimization (PSO), the BAT algorithm, and Quantum Particle Swarm Optimization (QPSO), to determine the best locations and sizes of DG to lower power losses, improve voltage profiles, reduce pollutant emissions, and lower overall generation costs in the distribution network. Due to the increasing usage patterns of DGs, including wind turbines, solar units, and fuel cells, the suggested methodologies are implemented and assessed on the standard modified IEEE 33-bus test system. A comparison analysis was conducted using the proposed method after four DG cases were taken into consideration. According to the simulation results, PSO power loss reductions ranged from 43.32% to 67.24%, BAT power loss reductions from 51.78% to 71.57%, and QPSO power loss reductions from 52.21% to 74.27% Throughout the test system network, the DGs' voltage profiles improved. The convergence characteristics demonstrate that increasing the number of DG units significantly enhances loss minimization. The comparison of the results with those of other optimization strategies showed the effectiveness of the suggested QPSO technique in optimal placement and sizing of DG.

1. Introduction

1.1. Background

The interest in Distributed Generation (DG) sources in recent times is increasing worldwide because of the rising power demand, high transmission losses, high carbon footprints, and greenhouse gas emissions produced by fossil-fuel-based energy generation sources [1]. According to the International Energy Agency (IEA), DG is defined as the "integration of multiple relatively small-power electrical energy sources into a local distribution network [2]. DG units are incorporated into power systems due to their economic, environmental, and technical benefits. Technically, they reinforce system dependability and power quality, lower system losses, improve voltage and frequency stability, increase energy efficiency, and relieve congestion in transmission and distribution networks. Economically, DG units ensure vital load security and optimal energy pricing while lowering facility upgrade costs, fuel costs, reserve requirements, and operating costs. In terms of the environment, they limit water outflow, cut waste production, and minimize pollution emissions [3,4]. The best location and size for DG units are crucial before integrating them into the utility grid. However, poor DG unit placement and sizing can increase power losses and possibly cause system instability; this kind of inefficient integration can greatly increase the cost of grid connection [5]. In DG technologies, the type, placement, size, and quantity of DG units are design factors that directly impact power losses and distribution network (DN) reliability. To guarantee the DN's dependable operation and utility grid stability, the integration of DG sources into the utility DN must be efficiently regulated and controlled [6,7]. The integration of DG units into power networks necessitates the use of appropriate optimization techniques. First, optimization enables them to improve the power system's performance and efficiency. Electric utilities can increase system performance, reduce energy losses, and boost overall operational efficiency by carefully choosing the best location and size for distributed generation

* Corresponding author.
E-mail address: saha@ukzn.ac.za (A.K. Saha).

https://doi.org/10.1016/j.rineng.2026.111420
Received 5 March 2026; Received in revised form 15 May 2026; Accepted 5 June 2026
Available online 6 June 2026

installations. This smart distribution of DGs guarantees their efficient use, resulting in a more productive and efficient power grid. Second, optimization methods minimize transmission losses, maximize energy generation and distribution in distributed generation, and provide chances for cost savings [8,9].

Additionally, the integration of renewable energy sources into the power grid depends heavily on optimization techniques. Researchers may maximize renewable energy generation and lessen dependency on fossil fuel-based power sources by figuring out where DGs, like solar panels or wind turbines, should be placed. This will help the transition to a more ecologically friendly and sustainable energy system. Particularly when integrating intermittent renewable energy sources, the distribution of DGs via optimization algorithms improves grid resilience and dependability, guaranteeing steady grid operations and lowering the risk of power outages [10,11]. Approaches for optimal DG integration in the literature can be broadly divided into two categories: heuristic or evolutionary techniques and conventional optimization methods. To solve DG placement and sizing issues, classical approaches—which are based on deterministic and non-deterministic mathematical formulations—usually use analytical models and convex programming techniques. These techniques are especially appropriate for systems where the underlying problem is convex and computationally manageable because they define the DG planning problem as a structured optimization assignment, which produces accurate and repeatable solutions. Furthermore, in large-scale, nonlinear DG planning situations where traditional mathematical optimization is difficult, heuristic or intelligent optimization techniques—which draw inspiration from natural processes—are frequently used. These methods are useful when the solution space is complicated or unclear since they can quickly locate near-optimal solutions with lower processing needs [12,13].

1.2. Literature review

Numerous studies have examined the advantages of DG allocation in distribution networks. This paper examines a number of suggested solutions for DG placement and sizing optimization, including programming techniques, a variety of mathematical and intelligent methodologies, analytical methods, and contemporary metaheuristic approaches inspired by natural processes. In a modified IEEE 13-bus distribution system, assessing the effects of photovoltaic (PV) and wind DG units under various scenarios and penetration levels, Salam et al. [1] examine the best location, size, and quantity of DG units using PSO to reduce power losses and improve reliability. The study examines how system performance is affected by DG unit unpredictability. The results highlight how effective DG integration can improve DN dependability and efficiency when renewable energy sources are present. The PSO algorithm is built in MATLAB R2018a, and the simulation studies are carried out using the ETAP software 19.0.1 edition. The simulation's results demonstrate that optimal solar and wind DG integration significantly improves load sharing, system reliability, and loss reduction at various DG uncertainty penetration levels. Taheri et al. [14] present a TLBO technique for efficient DG allocation in distribution systems that is based on Simulated-Annealing-Quasi-Oppositional (SAQO). The strategy seeks to reduce voltage losses, operating expenses, and greenhouse gas emissions by concentrating on wind turbines, solar power plants, and fuel cells. The proposed algorithm is implemented and evaluated on the IEEE 70-bus test system, with a comparative analysis conducted against other evolutionary methods such as Genetic Algorithm (GA), Particle Swarm Optimization (PSO), Honey Bee Mating Optimization (HBMO), and Teaching-Learning-Based Optimization (TLBO) algorithms. Results indicate that the proposed algorithm is effective in allocating the DGs. Statistical testing confirms significant results (probability < 0.1), indicating superior optimization capabilities for this specific problem. For optimal network reconfiguration with distributed generation (DG) integration, Yazin et al. [15] developed an Ant Lion Optimizer (ALO)-based method. Voltage stability, power losses, and power quality are some of the important distribution system performance parameters that are impacted by DG installation. ALO is an iterative exploration and exploitation metaheuristic that mimics the hunting behavior of antlions. The method is assessed under various load scenarios using the IEEE 69-bus test system. Three scenarios are examined: the initial network, network reconfiguration, and reconfiguration with DG integration. The outcomes demonstrate that the suggested approach successfully determines the best switch designs and DG locations, resulting in notable enhancements to the voltage profile and a decrease in power losses. Mezhoud et al. [16] use bio-inspired swarm optimization approaches to find the ideal location and size of renewable DG in a microgrid. The goal is to decrease power losses, improve voltage profiles, and increase system dependability and stability. With power loss reductions of 40.39% to 63.89% using PSO and 48.78% to 68.57% using the BAT algorithm, the results show good performance in comparison to current studies. In a similar vein, Prasad et al. [17] present a Multi-Objective Whale Optimization Algorithm (MOWOA) for the best placement of DG in the distribution network. Pareto-optimal compromise solutions are obtained by incorporating both equality and inequality requirements in the formulation. The proposed MOWOA is benchmarked against the Least Squares Fuzzy Satisfaction Approach (LSFA) and validated on IEEE 33- and 69-bus radial distribution systems. The results of the simulation show that MOWOA significantly improves the voltage profile while reducing power and economic losses. Derakhshan et al. [18] present a new index that is developed from the Power Stability Index (PSI) in order to ascertain the best location and dimensions for DG units in distribution networks. An analytical framework is created to assess how DG integration affects voltage stability, voltage profile, and power losses. Radial networks are subjected to a Co-Evolutionary Multi-Swarm PSO (CMPSO) algorithm that incorporates uncertainty related to load demand, solar generation, and wind power. The effectiveness of the suggested method was demonstrated by the validation conducted on the IEEE 33-bus and a realistic 274-bus distribution system. Ramadan et al. [19] present an Artificial Hummingbird Algorithm (AHA) for the best location and scaling of renewable DG in radial distribution systems while taking load demand and DG output uncertainties into account. The multi-objective optimization improves overall voltage stability while minimizing predicted total cost, emissions, and voltage variation. The IEEE 33-bus system and an actual 94-bus Portuguese network are used to validate the method. According to the findings, the suggested method offers efficient DG allocation, greatly lowering expenses, emissions, and voltage deviation while improving voltage stability. To find the best location and size for the DGs both before and after the radial network was reconfigured, Haider et al. [20] devised a multi-objective particle swarm optimization (MOPSO) technique. In an active distribution network, an ideal network layout with DG coordination eliminates power losses, raises voltage profiles, and enhances system efficiency, stability, and dependability. A penalty factor is also considered in order to minimize overall power loss and improve the voltage profile by considering the actual power system conditions. Using MATLAB software, the suggested algorithm is assessed on the IEEE-33 bus radial distribution system. According to the simulation results, the percentage power loss reduction was significantly improved, at 32% and 68.05%, respectively. In a similar vein, the system's minimum bus voltage improves by 4.9% and 6.53%, respectively. The findings of the comparison analysis demonstrated how well the suggested strategy worked to lower the distribution system's voltage deviation and power loss. Godha et al. [21] use the ant colony optimization (ACO) technique to minimize a techno-economic objective function in order to investigate the best way to integrate DG in distribution networks. The goal function considers expenses associated with grid power acquisition, DG installation, operation, and maintenance under various loading scenarios, as well as power loss, voltage variation, and operational cost indices. IEEE 33-bus and 85-bus radial distribution systems are used to validate the technique for solar and wind-based distributed generation. The success of the suggested strategy in comparison to current techniques is confirmed by the results, which show that appropriate DG placement greatly decreases power losses of 50–90%, improves voltage profiles of 6–13%, and produces notable cost savings of 14–39% The problem of growing the penetration of distributed energy resources (DER) and hosting capacity constraints in distribution systems is discussed by Taheri et al. [22]. It suggests a hybrid optimization strategy that combines honey-bee-mating optimization and teaching-learning-based optimization to find the best location for DERs while taking hosting capacity limitations and available resources into account. The technique uses fuzzy clustering in a multi-objective framework with voltage variation, cost, and power losses as objectives to enhance the quality of the solution. According to validation on the IEEE 70-bus system, the suggested method achieves faster convergence with roughly 9% and 22% reduction in calculation time compared to individual TLBO and HBMO algorithms, outperforming traditional methods in both accuracy and computational economy. Shaheen et al. [23] used the jellyfish search (JFS) method in power network reconfiguration (PNR) to improve distribution systems' operational reliability. System average interruption frequency index (SAIFI), system average interruption unavailability index (SAIUI), and total energy not supplied (TENS) are among the important reliability indices that are optimized within a multi-objective framework. An IEEE 33-bus system is used to validate the approach, and the findings demonstrate notable increases in reliability indices. The numerical findings show improvements of 36.44%, 34.11%, and 33.35% in SAIFI, SAIUI, and TENS over the starting condition. The JFS method outperforms the tuna swarm and tunicate swarm algorithms in terms of convergence characteristics and solution quality. Additionally, Shokouhandeh et al. [24] use the Lightning Search Algorithm (LSA) to find the best locations and sizes for distributed generation based on fuel cells, solar power, and wind in distribution networks in order to reduce power losses and enhance voltage profiles. Both steady load and load growth are considered by the method. Simulation findings on the IEEE 33-bus system prove the efficiency of the suggested technique in optimizing the goal function and show that load variations have a major impact on DG placement. In a similar vein, some other optimization techniques, such as the dragonfly algorithm [25] and Social Network Search (SNS) algorithm [26], are proposed by the researchers in the literature for obtaining optimal DG unit placement and sizing in DNs. In order to achieve power loss mitigation, reliability enhancement, voltage stability management, and other extra benefits in DNs, the effectiveness of all these optimization strategies is demonstrated by their use on various IEEE distribution test systems and genuine DNs as a case study. Furthermore, hybrid optimization techniques such as GWO and PSO [27] have been suggested for achieving the best location and size of DG units in power networks. These multi-objective strategies concentrate on reducing expenses, network losses, and enhancing the voltage profile.

1.3. Research gap and contributions

Although the DG placement issue in distribution systems has been successfully addressed by several researchers using optimization methods. Moreover, there is still a research gap that calls for more investigation. Grisales-Noreña et al. [28] investigate that most existing studies largely focus on analyzing the influence of optimal placement and sizing of DG units for power loss reduction and voltage profile enhancement in a radial DN. However, comparatively limited attention has been given to the simultaneous determination of the optimal placement, capacity, and type of DG units, particularly in grid-connected microgrid contexts, where their combined influence on overall DN performance requires detailed examination. In order to remove human decision-making bias, systematic and objective evaluation techniques must be used in the DG placement decision-making process. This illustrates yet another significant gap in the literature. According to a survey of the literature, most research treats DG placement as a single-objective optimization problem, ignoring the possible conflicts between several performance objectives. Even while some studies have presented Pareto fronts for multi-objective solutions [29], more sophisticated optimization methods that can offer greater computational accuracy and faster execution are still needed. Consequently, more research should be aimed toward the creation of highly efficient and precise multi-objective optimization algorithms that can better support decision-making in complicated DG integration scenarios. According to Malik et al. [30], the insufficient consideration of convergence behavior and computing time of current optimization algorithms constitutes a key research gap in the appropriate sizing and placement of distributed generation (DG) in grid-connected microgrids. Even though many researchers suggest sophisticated algorithms, many do not thoroughly assess their convergence stability, particularly in large-scale system configurations and a variety of operating situations. Furthermore, a number of methods increase computational complexity and execution times in order to attain high solution accuracy. Moreover, there aren't many optimization frameworks that can provide dependable global optimality, quick convergence, and a lighter computing load all at once. As a result, this study creates scalable and effective optimization techniques that balance computational economy and convergence speed in contemporary microgrid design.

In this research, three proposed optimization frameworks, such as Particle Swarm Optimization (PSO), Quantum Particle Swarm Optimization (QPSO), and an algorithm inspired by nature, like the BAT algorithm, are analyzed for the simultaneous sizing and location of DG units in a grid-connected microgrid to evaluate their operational performance on DN, while demonstrating high solution accuracy and competitive computational efficiency. Furthermore, this research presents the idea of storing Pareto optimal solutions discovered throughout the search process in an external cache. Finding workable non-dominated solutions that provide the ideal trade-off between objective functions is the main goal of applying the Pareto principle to the approaches. The proposed approach significantly reduces the need for direct human engagement by clustering the multi-objective optimum solutions using recommended weight factors, and a fuzzy decision-making strategy further optimizes the decision-making process with the goals of lowering power losses, improving voltage profiles, increasing dependability, reducing pollutant emissions, and lowering overall generation costs. In this study, a modified 33-bus test system is used to assess the performance of the suggested optimization framework for DG location and sizing. The performance of the suggested algorithms is tested and compared with other widely recognized optimization techniques. Through this comparative analysis, the effectiveness and efficiency of the suggested algorithms are tested, and their competitiveness among established optimization strategies is determined.

The following is a summary of the research's contributions:

- Create a grid-connected microgrid model based on DG that incorporates fuel cells, solar PV, wind, and the utility grid to improve the voltage profile of the modified IEEE 33-bus system, minimize losses, and provide energy efficiency.
- Outlines optimization methods for the best location, capacity, and kind of DG units in the context of grid-connected microgrids to assess the distribution network's operational performance.
- Presents the validation performance and convergence with computational accuracy of the proposed optimization framework for sizing and positioning of DG across a 33-bus distribution network.
- Presents a comparative examination of integrating three well-established optimization methods to boost energy efficiency and enhance the grid's overall performance and stability.
- Presents a multi-objective clustering function employing a suggested weight factor and fuzzy decision-making strategy to bypass the human decision-making interface for selecting the best-compromised solution.

This paper's remaining sections are organized as follows. Section 2 presents the modelling of DGs based grid connected on the modified 33 IEEE bus test system. Section 3 presents the economic specification of the implementation of each DG on the modified 33 IEEE bus test system. In Section 4, the ideal placement of DG is formulated mathematically, with particular attention to the assessment of total power losses in the grid-connected microgrid. The suggested optimization technique's performance features in identifying the ideal DG location and size are covered in Section 5. Section 6 shows and evaluates the outcomes to confirm the efficacy of the suggested approaches. Finally, in Section 7, the main research conclusions are summarized, and suggestions for further research are provided.

2. Architecture of DG-based grid-connected microgrid

A typical distribution network model of DG integration is shown in Fig. 1. Based on their capacity to interchange both active and reactive power with the grid, Huy et al. [31] divided DG technologies into the following four categories. Type 1 DG units can only provide the system with active power. Microturbines (MT), Fuel Cells (FC), and PV systems. Type 2 DG units, such as synchronous generators and Doubly-Fed Induction Generators (DFIG) in wind energy applications, can provide both active and reactive power at the same time. Type 3 DG units, like synchronous compensators and gas turbine-driven systems, only supply the grid with reactive power. Lastly, Type 4 DG units, such as induction generators frequently used in wind farms, produce active power but need reactive power from the network to function. The optimal sizing of DG-based grid-connected microgrids must account for the stochastic behavior of both generation and load to achieve significant loss reduction. Consequently, the size procedure becomes a complex planning process that is impacted by several technical limitations, energy balancing requirements, and investment costs. For a modified IEEE 33-bus system, a DG-based grid-connected microgrid model was constructed as shown in Fig. 2. The system topology is mostly composed of solar PV, FC, WT, and the utility grid. The optimal DG position and size are investigated by analyzing and modifying the system through energy efficiency planning. The size of the DGs is influenced by their availability, cost, intermittency, and the choices made for demand forecasting and energy management system (EMS) strategies. The system was designed with the following constraints:

- The voltage (V) range is contained within the designated higher V_{ul} (1.05 $p.u.$) and lower V_{ll} (0.95 $p.u.$) limits. The system has a line-to-line voltage rating of 415 V

$$V_{ll} < V < V_{ul} \tag{1}$$

- The frequency (f) is kept within the predetermined upper f_{ul} (50.5 H_Z) and lower f_{ll} (49.5 H_Z) bounds. The system has a 50 H_Z rated frequency.

$$f_{ll} < V < f_{ul} \tag{2}$$

- The line limits are always followed, that is, the current flowing through the lines (I_{line}) should be less than or equal to the rated current (I_{rated}).

$$I_{line} \leq I_{rated} \tag{3}$$

2.1. DG modeling

In the system modeling stage, each microgrid component is ideally designed by considering resource availability data and essential economic criteria. In order to ensure feasible system performance, the sizing technique is developed within a set of predetermined technical, operational, and financial restrictions.

2.1.1. Solar PV generation

The size of the array and the solar modules' conversion efficiency are the main factors that define a solar PV array's output power. Under the premise of continuous operation at the maximum power point (MPPT) controller, the PV output can be modeled as a function of solar irradiation. The solar PV power generation is expressed in Eq. (4):

$$P_{PV} = \eta_{PV} * A * G\{1 + \gamma(T_0 - 25)\} \tag{4}$$

where, P_{PV} stands for the output power of the PV array (kW), η_{PV} is the conversion efficiency of the PV module, A is the total surface area of the PV array (m^2), G represents the solar irradiance incident on the PV surface (W/m^2), γ is the temperature coefficient of power for the PV module (°C), and T_0 represents the operating cell temperature of the PV module (°C), with 25 °C serving as the reference standard test condition (STC) [32].

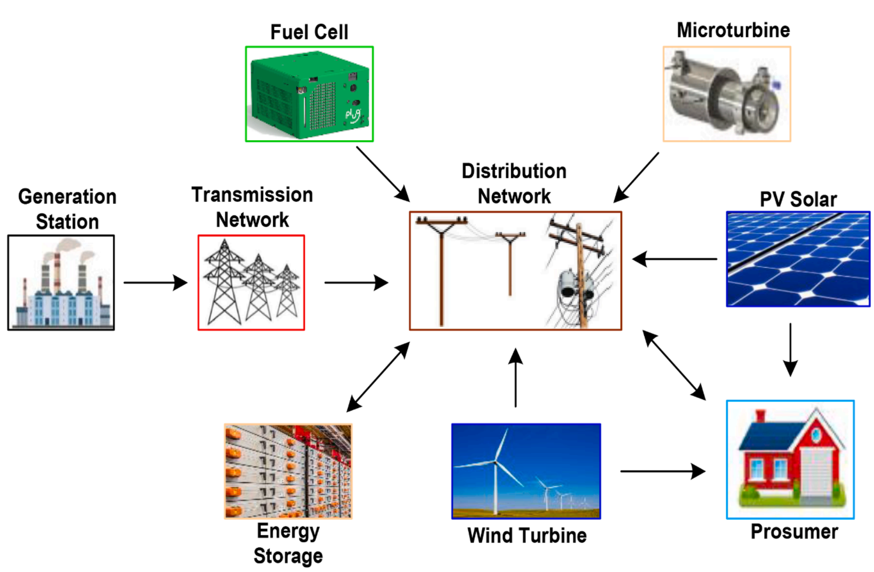

Fig. 1. Typical model of DG integration in a distribution network.

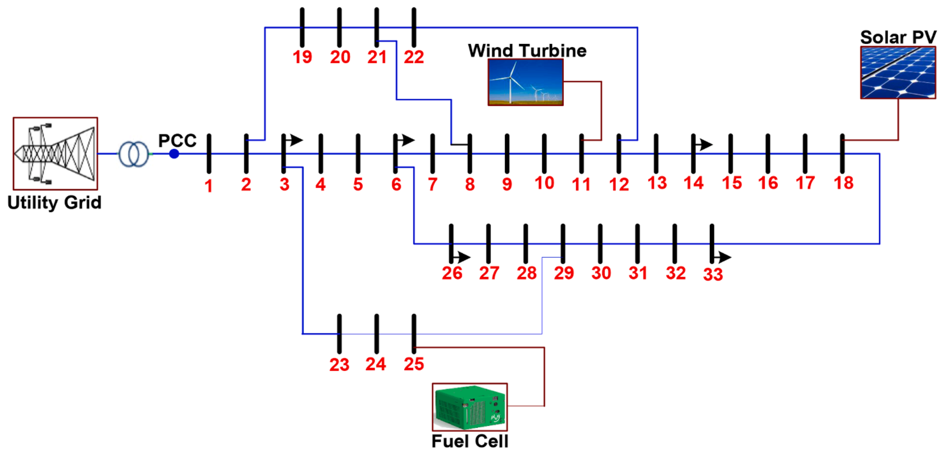

Fig. 2. An illustration of a modified IEEE 33-bus system with DGs based on a grid-connected microgrid.

2.1.2. Wind turbine

Wind power is intrinsically stochastic, as it is produced by converting the kinetic energy of wind through turbine components such as the tower, blades, and rotor. Consequently, the available wind power greatly depends on ambient wind speed, which varies with height. This variance is computed by projecting the recorded wind speed to the turbine hub height using the power-law wind profile given in Eq. (5).

$$\frac{\upsilon}{\upsilon_0} = \left(\frac{h}{h_0}\right)^{\alpha} \tag{5}$$

where, υ stands for the wind speed at the turbine hub height (m/s), υ_0 is the reference wind speed measured at height $h_0(m/s)$, h is the hub height of the wind turbine (m), h_0 is the reference wind speed measurement height (m), and α represents the exponential wind shear. Moreover, after correcting the wind speed to the turbine hub height, the mechanical power output of a wind turbine is predicted using its characteristic power curve. Key operational constraints, such as cut-in, rated, and cut-out wind speeds, determine the production. The wind turbine power curve mathematical model is expressed in Eq. (6).

$$P_{WT}(\upsilon) = \begin{cases} 0 & \upsilon < \upsilon_{ci} \\ P_{rated}\left(\dfrac{\upsilon - \upsilon_{ci}}{\upsilon_r - \upsilon_{ci}}\right)^3 & \upsilon_{ci} < \upsilon < \upsilon_r \\ P_{rated} & \upsilon_r \le \upsilon \le \upsilon_{co} \\ 0 & \upsilon > \upsilon_{co} \end{cases} \tag{6}$$

where, P_{WT} is the power output of the wind turbine at wind speed (kW), υ_{ci} represents the cut-in wind speed: minimum wind speed needed for power generation (m/s), υ_r represents the rated wind speed: the wind speed at which the turbine generates its nominal rated power (m/s), υ_{co} represents the cut-out wind speed: the wind speed above which the turbine shuts down to prevent mechanical damage (m/s), and P_{rated} is the rated maximum output power of the wind turbine (kW) [32]. Weibull distribution is frequently used to depict the temporal variations in wind speed. The Weibull probability distribution function can be expressed as follows:

$$f_{WT} = \begin{cases} \dfrac{\beta}{\gamma} * \left(\dfrac{\upsilon}{\gamma}\right)^{\beta-1} * e - \left(\dfrac{\upsilon}{\gamma}\right)^{\beta} & \upsilon \ge 0 \\ 0 & Otherwise \end{cases} \tag{7}$$

2.1.3. Fuel cell

Fuel cells are clean energy conversion devices that use an electrochemical reaction to produce direct current (DC) power from chemical energy. They offer various advantages, including high efficiency, simple operation, low maintenance requirements, and carbon-neutral performance when supplied with green hydrogen [33]. In a microgrid powered by renewable energy, excess electrical power is fed into an electrolyzer that uses DC electrolysis to create hydrogen. The hydrogen is then stored and used as fuel in the fuel cell, allowing excess electricity to be converted into storable energy. The output power from the electrolyzer to the hydrogen tank is expressed as follows:

$$P_{out-H_2(t)} = P_{in-ele} * \eta_{ele} \tag{8}$$

where, $P_{out-H_2(t)}$ and P_{in-ele} are the output and input power of the electrolyzer, and η_{ele} is the electrolyzer efficiency. The calculation of the fuel cell plant's overall power output is presented in Eq. (9).

$$P_{FC}(t) = P_{H_2-FC} * \eta_{FC} \tag{9}$$

where, P_{H_2-FC} is the FC input power and η_{FC} is the overall FC efficiency.

2.1.4. Energy storage and state of charging

In microgrids, BESS play a significant role in managing the intermittency of renewable energy sources and aiding peak-load shaving. A BESS's needed storage capacity can be represented as follows:

$$C_{BESS} = \frac{AD * P_{Load}}{\eta_{inv}\eta_{BESS} * DoD} \tag{10}$$

where, C_{BESS} represents the necessary BESS capacity (kWh), AD represents the autonomy time (hours), P_{Load} represents the average load demand to be supported (kW), η_{inv}, η_{BESS} represent the round trip efficiency of the inverter and battery, and DoD is the permitted depth of discharge battery. Additionally, the surplus energy is used to charge the BESS when the microgrid's total power generation surpasses the load requirement. The power required to charge a battery can be written as:

$$P_{BESS}(t) = P_{PV}(t) + P_{Wind}(t) + P_{FC}(t) - \frac{P_{Load}(t)}{\eta_{inv}} \tag{11}$$

Thus, $P_{BESS}(t)$ is the charging power of the BESS at time (t), $P_{PV}(t)$, $P_{Wind}(t)$, $P_{FC}(t)$ are the power outputs from the PV array, WT, and FC, respectively, $P_{Load}(t)$ is the microgrid load demand. Thus, the fundamental factor influencing battery performance in BESS operation is state of charge (SoC), which is based on the excess or shortfall of power produced by RESs relative to the demand. The SoC of the battery needs to be constantly monitored to guarantee that the battery does not enter harmful cycles of overcharge or deep discharge. The SoC of the battery determines how much power DG requires, and a battery with a higher SoC requires less power, as expressed in Eq. (12).

$$20\% \le SoC \le 80\% \tag{12}$$

The charging duration is a significant aspect for optimizing the cost, as it is another signal of the power consumption from the standpoint of the DG-based grid-connected microgrid [34,35].

2.1.5. Total DG power demand

The DG power demand ($P_{DG,demand}$) is evaluated as the sum of the generations from the solar PV, WT, and FC. The DG power demand can be expressed as:

$$P_{DG,demand} = \sum_{t=1}^{n} (P_{PV}(t) + P_{wind}(t) + P_{FC}(t)) \tag{13}$$

$P_{PV}(t)$, $P_{wind}(t)$, and $P_{FC}(t)$ represent the power produced at time 't' generated by the solar PV system, WT, and FC. The power extracted drawn from the grid (P_{grid}) can be expressed as:

$$P_{grid} = \begin{cases} 0, \ if \ P_{DG,gen} = P_{total,\ dem} \\ P_{total,\ dem} - P_{DG,gen} \ if \ P_{DG,gen} \neq P_{total,dem} \end{cases} \tag{14}$$

When DG output surpasses load demand, the extra power is fed into the grid. The percentage of power used in relation to total generation is known as the DG usage ratio, and it can be represented as follows:

$$\%DG = \frac{P_{DG,gen}}{P_{DG,gen} + P_{grid}} \times 100 \tag{15}$$

2.2. DG uncertainty modeling

Uncertainty in grid-connected microgrids is mostly caused by the sporadic nature of renewable energy sources and fluctuations in load demand. Stochastic programming and scenario-based modeling techniques are frequently used in the IEEE 33-bus system to accurately depict these uncertainties. The three (3) uncertainty factors—solar PV, wind turbines, and fuel cells—are assumed and taken into account in this study. The uncertainty modeling parameters are forecasted using the historical recorded dataset and the stochastic planning technique described in Refs. [36]. The parameter sensitivity analysis for the uncertainty modeling is shown in Table 1. The following model represents the uncertainties in solar PV, WT, and FC power output:

$$P_{PV,t,s} = P^{f}_{PV,t} + \Delta P_{PV,t,s} : \ t = 1, \ldots, N_T; \ s = 1, \ldots, N_s \tag{16}$$

$$P_{WT,t,s} = P^{f}_{WT,t} + \Delta P_{WT,t,s} : \ t = 1, \ldots, N_T; \ s = 1, \ldots, N_s \tag{17}$$

$$P_{FC,t,s} = P^{f}_{FC,t} + \Delta P_{FC,t,s} : \ t = 1, \ldots, N_T; \ s = 1, \ldots, N_s \tag{18}$$

where, $P^{f}_{PV,t}$, $P^{f}_{WT,t}$, $P^{f}_{FC,t}$, $\Delta P_{PV,t,s}$, $\Delta P_{WT,t,s}$, and $\Delta P_{FC,t,s}$, are forecasted output power of PV, WT, and FC with their forecast errors respectively. N_T and N_s are time interval quantities, and scenario quantities are chosen for the uncertainty model. The uncertainty variables modeled, are simulated using MATLAB software. The observed data X, and the predicted data X^* can be justified using mean square error (MSE), root mean square error (RMSE), and mean absolute percentage error (MAPE) as expressed as follows:

Table 1
Uncertainty modeling parameters sensitivity analysis.

Uncertainty	Statistical model	Parameters	Description
$\Delta P_{PV,t,s}$	Beta distribution	$\alpha = 2, \beta = 5$	Wind speed variability
$\Delta P_{WT,t,s}$	Weibull distribution	$k = 2, c = 13.5\ m/s$	Solar irradiance variability
$\Delta P_{FC,t,s}$	Gaussian distribution	$\sigma = 0.05$P, $\mu =$ P_rated	Output fluctuation
Load demand	Normal distribution	$\sigma = 20\%$, $\mu =$ P_load	Load uncertainty
Scenarios	Monte Carlo	N = 1000	Random operating condition

$$MSE = \frac{1}{n} \sum_{i=1}^{n} (X_i^* - X_i)^2 \tag{19}$$

$$RMSE = \sqrt{\frac{1}{n} \sum_{i=1}^{n} (X_i^* - X_i)^2} \tag{20}$$

$$MAPE = \frac{1}{n} \sum_{i=1}^{n} \left| \frac{X_i^* - X_i}{X_i} \right| \tag{21}$$

For testing and training in the prediction process, wind turbines, solar PV, and FC are simulated using the Weibull distribution, Beta distribution, and Gaussian process modeling. The uncertainty was effectively represented by the artificial neural network (ANN) technology.

The uncertainty modeling of solar PV generation using ANN prediction compared with actual solar PV data is shown in Fig. 3. The PV output gradually increases after 5 h, peaks at about 9 kW around 11 h, and then decreases toward zero in the evening period. The close agreement between the ANN output and the actual PV data indicates the strong prediction capability of the proposed model; this accuracy is validated by the low MSE of 0.015 and RMSE of 0.123, indicating the efficacy of the ANN model for solar PV uncertainty forecasting in microgrid applications. After five hours, the PV output gradually rises, peaks at about 9 kW at eleven hours, and then falls to zero in the evening. The great prediction capacity of the suggested model is demonstrated by the good agreement between the ANN output and the real PV data. The low MSE of 0.015 and RMSE of 0.123 corroborate this accuracy and show how useful the ANN model is for solar PV uncertainty predictions in microgrid applications. Furthermore, the uncertainty modeling of wind turbine generation using ANN prediction is compared with actual wind turbine data in Fig. 4. The wind power output shows continuous fluctuations throughout the 24-hour period due to varying wind conditions, with generation increasing significantly after 10 h and reaching values above 5 kW during later hours. The ANN output closely follows the actual wind turbine profile, demonstrating strong prediction capability and effective tracking of wind power variations. The low error values of MSE = 0.024, RMSE = 0.154, and MAPE = 0.104 validate the accuracy and dependability of the suggested ANN-based uncertainty forecasting model for microgrid applications. Due to fluctuating wind conditions, the wind power output fluctuates continuously over the course of a 24-hour period, with generation rising sharply after 10 h and surpassing 5 kW in later hours. Strong prediction ability and efficient tracking of wind power fluctuations are demonstrated by the ANN output, which closely resembles the real wind turbine profile. The accuracy and dependability of the suggested ANN-based uncertainty forecasting model for microgrid applications are confirmed by the low error values of MSE = 0.024, RMSE = 0.154, and MAPE = 0.104. The Fig. 5 displays the fuel cell's uncertainty modeling using ANN prediction in comparison to actual fuel cell data. The fuel cell production first drops to a minimum around hour five, then progressively rises to a peak of about 540 kW around hour fifteen before starting to decline again toward the end of the time. The great prediction ability of the suggested model is demonstrated by the good agreement between the ANN output and the actual fuel cell data. The low MAPE of 0.011, RMSE of 5.686, and MSE of 32.332 corroborate this accuracy and demonstrate the effectiveness of the ANN model for fuel cell uncertainty forecasting in microgrid applications.

3. Test bed: modified IEEE 33 bus system

This research is conducted using a modified IEEE 33-bus test system that integrates the utility grid and DG units. The IEEE 33-bus system serves as the base network, while the system voltage, frequency, and line parameters are adjusted in accordance with the standards reported in Gautam et al. [37]. There are 33 branches in the system. The utility grid

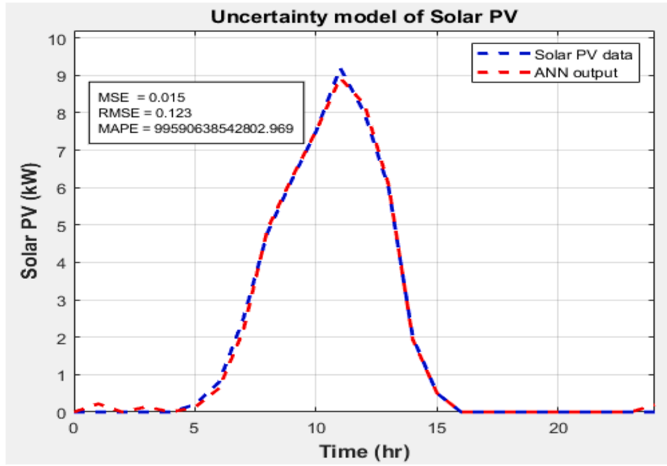

Fig. 3. Uncertainty model of solar PV.

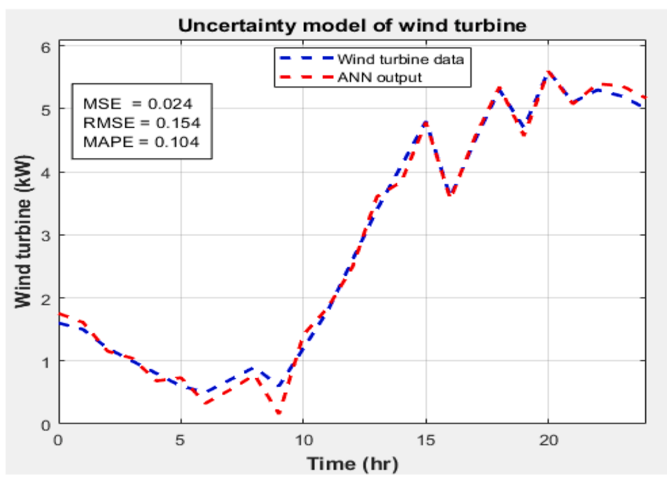

Fig. 4. Uncertainty model of wind turbine.

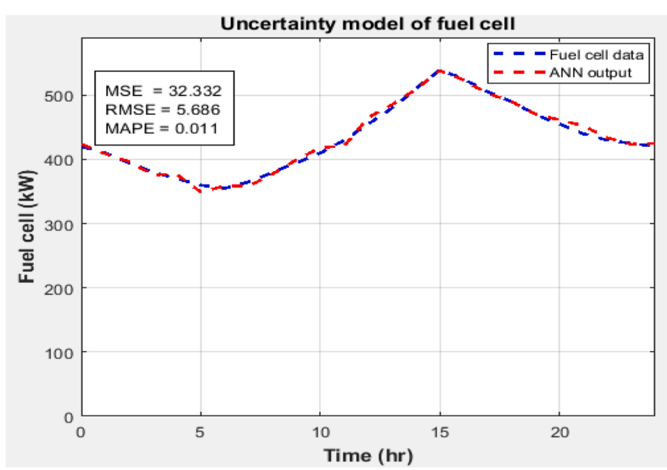

Fig. 5. Uncertainty model of fuel cell.

at node 1 is regarded as a swing bus with a frequency of 50 H_Z and a line-to-line rating of 415 V A wind turbine rated at 30 kW is located at bus 11. The wind turbine's power output is directly correlated with wind speed. The maximum and nominal wind speeds were determined to be 15 m/s and 13.5 m/s, respectively. In a similar vein, bus 18 offers the 35-kW solar PV system. At a temperature of 25 $^{\circ}C$ and an irradiation of 1000 W/m^2, the rated output power was achieved. Throughout the day, the irradiance profile changed, reaching its highest value at noon. Before sunrise and after nightfall, the irradiance reached zero. This analysis assumed that WT could always provide power continuously. The microgrid is powered by the main grid and has a 600-kWh installed capacity for backup energy storage. The depth-of-discharge (DoD) limit is set at 80% to ensure battery longevity. Bus 25 is equipped with a 35-kW fuel cell. In this analysis, the fuel cell's output is regarded as constant during 24 h. Within the system were five loads. They are located at nodes 3, 6, 14, 26, and 33, and their respective ratings are 1 kW, 4 kW, 6 kW, 8 kW, and 12 kW Table 2 displays their economic specifications for the DGs that have been implemented. In this research, the installation of the three DGs was expected to improve the system's power quality, improve the voltage profile, lower overall operating cost, reduce power losses, and lower pollutant emissions. The locations are chosen in accordance with Gautam et al. [37], which proposes the optimal locations for the placement of the DG in the IEEE 33-bus system based on the ampacity limit, voltage sensitivity factor (VSF), and voltage stability index (VSI).

4. Problem formulation for DG placement

This section assesses how changes in bus injection power affect the distribution network's overall power losses since voltage fluctuations affect how power flows behave and the ensuing losses. The overall power losses can be computed using the total amount of injected active power in each bus.

$$P_{loss} = \sum_{i=1}^{N_b} \sum_{j\in a_i} V_i V_j \left[G_{ij} cos(\theta_i - \theta_j) + B_{ij} sin(\theta_i - \theta_j)\right] \tag{22}$$

In (22), the power loss derivation is provided as follows:

$$\frac{\partial \boldsymbol{P_{loss}}}{\partial \boldsymbol{V_i}} = \sum_{i=1}^{N_b} \sum_{j\in a_i} \boldsymbol{V_i V_j}\left[\boldsymbol{B_{ij} cos}(\boldsymbol{\theta_i} - \boldsymbol{\theta_j}) - \boldsymbol{G_{ij} sin}(\boldsymbol{\theta_i} - \boldsymbol{\theta_j})\right] \tag{23}$$

$$\frac{\partial \boldsymbol{P_{loss}}}{\partial \boldsymbol{\theta_i}} = \sum_{i=1}^{N_b} \sum_{j\in a_i} \boldsymbol{V_i V_j}\left[\boldsymbol{G_{ij} cos}(\boldsymbol{\theta_i} - \boldsymbol{\theta_j}) + \boldsymbol{B_{ij} sin}(\boldsymbol{\theta_i} - \boldsymbol{\theta_j})\right] \tag{24}$$

where $\boldsymbol{V_i}$, $\boldsymbol{\theta_i}$, $\boldsymbol{V_j}$, and $\boldsymbol{\theta_j}$ are the magnitude and angle voltages at bus $\boldsymbol{i}$ and $\boldsymbol{j}$, respectively, and $\boldsymbol{P_{loss}}$ is the overall power loss. $\boldsymbol{G_{ij}}$ and $\boldsymbol{B_{ij}}$ represent the network's conductance and susceptibility, $\boldsymbol{a_i}$ is the group of buses connected at bus $\boldsymbol{i}$, and $\boldsymbol{N_b}$ is the total number of buses.

4.1. Loss sensitivity index

The loss sensitivity index (LSI) offers a methodical way to choose the best locations for DG. In order to guide effective DG allocation, the LSI measures each bus's contribution to total system losses and assesses how sensitive these losses are to power compensation. In order to determine the best locations for DG placement, the active and reactive power losses at each bus are assessed, and buses with the largest loss contributions are given precedence. The largest reduction in overall system losses is achieved by deploying DG units at these high-loss areas. The LSI technique simplifies the optimization process, lessens the computing load, and lowers the costs associated with DG implementation by narrowing the search to the most significant buses [38]. The LSI values serve as bus location coefficients (BLCs) in this research, giving a numerical representation of the optimal locations for DG integration.

Table 2
Economic specification of the implemented DG.

DG Type	Solar PV	WT	FC	BESS
Rated capacity (kW)	35	30	35	600
Capital cost ($\$/kW$)	1000	900	720	1500
Fuel cost ($\$/kW$)	0	0	1.5	0
Cost of operation and maintenance ($\$/kW$)	0.5	0.5	0.1	0.1
Life-time (year)	20	20	10	10

$$LSI_i = BLC_i = \omega \frac{\partial P_{loss}}{\partial P_i} + (1-\omega)\frac{\partial P_{loss}}{\partial Q_i} \tag{25}$$

In this case, ω is the weight factor that depends on the network's (r/x). The ratio of feeders to ttransformers in the DN, as well as the resistance and reactance (r/x), vary greatly. According to this method, the weight factor ω should be determined independently for every bus in DNs with a wide range of (r/x) ratio.

4.2. Objective function

The suggested objective functions and realistic limitations that make up the problem's mathematical formulation are presented in this section. The active power loss is the research objective function, and it can be stated as follows:

$$P_{loss} = \sum_{i=1}^{N_b} R_i I_i^2 \tag{26}$$

where, I_i and R_i are the current and line resistance. The network X/R ratio can be used to determine reactive power loss from active power loss because they are proportional to branch reactance. A common X/R ratio of about 1.25 is assumed for the IEEE 33-bus distribution system.

4.2.1. Total generation cost

Based on the parameters listed in Table 1, this research develops the cost function for each unit in accordance with the economic considerations of DG. The following is the mathematical model for total generation costs:

$$f_1(\chi) = \sum_{i=1}^{N_{PV}} C_{PV}(P_{PV}) + \sum_{j=1}^{N_{FC}} C_{FC}(P_{FC}) + \sum_{k=1}^{N_{WT}} C_{WT}(P_{WT}) \tag{27}$$

$$F_1(\chi) = \min[f_1(\chi)] \tag{28}$$

The function of χ is represented by the position and power vectors of FC, PV, and WT.

4.2.2. Bus voltage deviation

The bus voltage deviation is measured using the following expression:

$$f_2(\chi) = \sum_{m=1}^{N_{bus}} \frac{|V_{nom} - V_r|}{V_{nom}} \tag{29}$$

$$F_2(\chi) = \min[f_2(\chi)] \tag{30}$$

where V_{nom} is the nominal bus voltage, and V_r is the actual voltage magnitude at bus m. This index is used to evaluate the distribution network's overall voltage profile quality by quantifying the extent to which bus voltages differ from their nominal values.

4.2.3. Power losses

In order to reduce the overall power losses across all network lines, the third goal function for the DG placement problem is developed. It is expressed as:

$$f_3(\chi) = \sum_{a=1}^{N_{lt}} \sum_{b=1}^{N_{nb}} \left(R_m I_m^2 \Delta t\right) \tag{31}$$

$$F_3(\chi) = \min[f_3(\chi)] \tag{32}$$

where R_m denotes the resistance of line m, I_m is the corresponding line current magnitude, and Δt represents the evaluation time interval.

4.2.4. Emission

The overall amount of greenhouse gas emissions from fossil fuel-based thermal units, including sulfur oxides (SO_x) and nitrogen oxides (NO_x). Assuming that BESS emissions converge to zero during regular operation, each unit's emission function is written as follows:

$$E_t = \sum_{n=1}^{N_{DG}} E_n(P_n) \tag{33}$$

$$E_n(P_n) = a_n P_n^2 + b_n P_n + g_n + x_n \exp(9\ In\ P_n) \tag{34}$$

$$f_4(\chi) = \mathrm{E}_{t_{FC}} + \mathrm{E}_{t_{WT}} + \mathrm{E}_{t_{PV}} \tag{35}$$

The coefficients of emission are as follows: a_n, b_n, g_n, and x_n, respectively.

4.3. Constraints

In DN, stable operation requires that the bus voltages stay within allowable bounds. Throughout the optimization process, these restrictions ensure that the voltage profile stays within legal and operational requirements. The voltage restriction for every bus can be written as follows:

$$V_i^{min} \le V_i \le V_i^{max} \tag{36}$$

In this case, V_i represents the voltage magnitude at bus i, and the lower and upper acceptable voltage limits are indicated by V_i^{min} and V_i^{max}, respectively.

4.3.1. Power balance constraints

To maintain system stability, the DN's active power balance needs to be kept constant. By imposing this limitation, the total power generated is guaranteed to equal the sum of the system losses and load demand.

$$\sum_{i=1}^{N_G} P_{gi} + \sum_{k=1}^{N_{DG}} P_{DG_k} = P_D + P_{Loss} \tag{37}$$

where, P_{gi} is the active power generated by the i th conventional generator, P_{DG_k} is the active power supplied by the k-th DG units, P_D denotes the total active power demand, and P_{Loss} represents the total active power losses in the network.

4.3.2. Constraints of DG capacity limit

By ensuring that DG units run within their rated capabilities, this constraint helps to preserve system stability and avoid overloading.

$$P_{DG}^{min} \le P_{DG} \le P_{DG}^{max} \tag{38}$$

P_{DG}^{min} and P_{DG}^{max} represent the DG unit's minimum and maximum permitted active power levels, respectively.

5. Optimization techniques

This research examines three optimization methods for DG placement and sizing: the BAT algorithm, PSO, and QPSO. These methods are more computationally efficient than nonlinear programming. The integration aims to improve convergence precision, increase the optimization population, and avoid premature convergence to a local minimum [39]. The PSO algorithm is chosen as the starting point for additional improvement because of its ease of implementation and simplicity in parameter adjustment. PSO is effective for multi-objective optimization, has excellent performance in non-linear power flow circumstances, and has good global search capabilities. PSO prevents premature convergence as compared to many conventional optimization techniques. However, PSO faced trouble handling extremely constrained issues and lacks a powerful exploitation mechanism for precise local search and fine-tuning of optimal solutions. The BAT algorithm method was selected because it is effective at exploring search spaces through adaptive frequency and velocity modifications and solving complex multi-modal optimization problems. It reduces the likelihood of premature convergence by offering an efficient balance between exploration and exploitation. However, the algorithm is still getting stuck in local minima, especially in extremely complex search spaces without parameter fine-tuning. QPSO, an upgraded variant of classical PSO developed from quantum physics principles. QPSO offers a better balance between exploration and exploitation, increased optimization accuracy, faster convergence for large-scale systems, and enhanced global search capabilities. Its dynamic swarm behavior and quantum-inspired operators help it overcome common problems that classical algorithms have, like managing complex, multi-modal, and non-linear objective functions. QPSO enables more comprehensive solution space search and efficient multi-objective optimization by combining swarm intelligence and quantum-inspired ideas. By employing quantum superposition and entanglement, QPSO offers an unmatched capacity to examine several solution spaces simultaneously, significantly accelerating the convergence toward near-optimal energy dispatch algorithms [40,41]. The comparative optimization flowcharts for optimal sizing and location of DG units in a modified IEEE 33-bus test system are presented in Fig. 6.

5.1. BAT algorithm

Xin-She Yang first presented the bat algorithm in 2010. It is a bio-inspired optimization method that imitates the echolocation behavior of microbats. The microbat is the bat species that uses echolocation the most frequently. To find prey, recognize things, and avoid obstacles, a bat will use sonar. Echoes are created when these sonar sounds bounce back from an object. Bats determine the size of an object by measuring the time interval between the production of an echo signal and its observed position. Depending on how close they are to their food, bats dynamically modify the volume and pulse emission rate of their signals during the search phase [42,43]. The Bat algorithm is implemented under the following idealized assumptions:

- All bats are assumed to use an echolocation mechanism to find prey in their surroundings, identify barriers, avoid feasible regions, and distinguish between potential solutions based on their fitness values.
- Each bat is initialized with a frequency $f_i \in [f_{min}, f_{max}]$, a variable loudness A_0, wavelength λ, random velocity v_i, and position x_i which define its movement within the solution space.
- As the search progresses and a bat approaches the target, the pulse rate rises, the loudness A_0 falls from an initial high value to a predetermined minimum value A_{min}.
- Bats use a random walk around the current best solution to increase exploitation and improve solution accuracy when a local search mechanism is triggered based on the pulse emission rate.

Mathematically, each bat's frequency is first modified as follows:

$$f_i = f_{min} + (f_{max} - f_{min}) * rand \tag{39}$$

Next, the i-th bat's velocity is modified based on:

$$v_i^t = v_i^{t-1} + \left(x_i^{t-1} - x^*\right) * f_i \tag{40}$$

The bat's new position is determined by:

$$x_i^t = x_i^{t-1} + v_i^t \tag{41}$$

Where, x_i^t and v_i^t denote the current position and velocity of the i-th bat at iteration t, and x^* represents the current global best (gbest) solution found by the population. A new solution locally centered around that solution is then produced by a random walk in Eq. (42).

$$x_{new} = x_{best} + \varepsilon A^t \tag{42}$$

Thus, A^t is the average loudness of all bats in the current iteration, while ε represents a random value between [−1, 1]. For every iteration

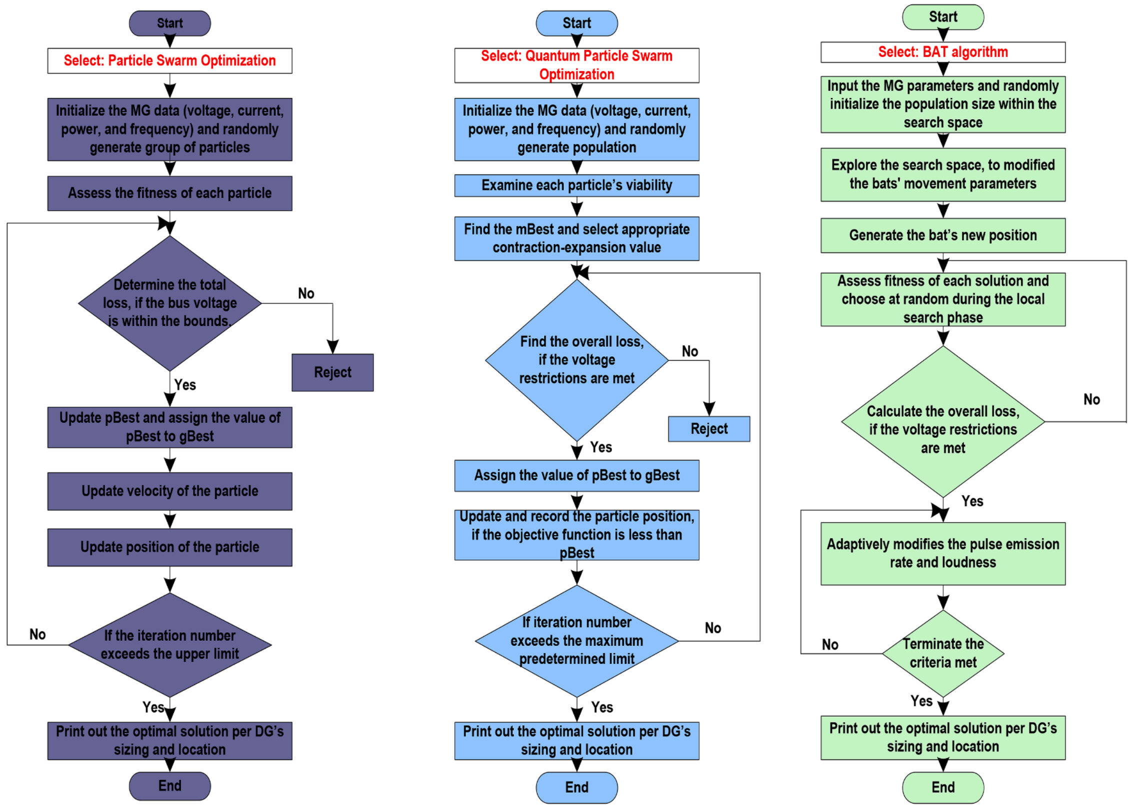

Fig. 6. Comparative optimization flowcharts for the sizing and location of DGs across the modified IEEE 33-bus test system.

update, the pulse emission rate and loudness of all bats can be expressed as:

$$A_i^{t+1} = \alpha A_i^t \tag{43}$$

$$r_i^{t+1} = r_i^0[1 - \exp(-\gamma t)] \tag{44}$$

Since α and γ are constants that regulate the loudness and pulse rate, their values are taken to be 0.9.

5.1.1. *Steps for the BAT algorithm*

This section describes how to solve the optimal position and scale of DG in a grid-connected microgrid using the suggested bat algorithm. The steps listed below are described as:

Step 1: Input system data

Input network data, including bus/line parameters, DG limits, voltage constraints, and load demand for the microgrid.

Step 2: Initialization

The bat population is randomly initialized within the search space, typically ranging between 10 and 40 agents. In this work, a population size of 20 is chosen. The objective function is used to assess each bat's fitness, and changes in loudness, pulse emission rate, and velocity are used to iteratively update the bats' locations.

Step 3: Movement of bats

To efficiently explore the search space, the bats' movement parameters are modified with each iteration by using Eqs. (39) to (42).

Step 4: Local search by random walk

To increase exploitation, one of the best solutions is chosen at random during the local search phase by using Eq. (42).

Step 5: The pulse emission and loudness

By using Eqs. (43) & (44), the bat algorithm adaptively modifies the pulse emission rate and loudness A_i as bats get closer to a promising solution. A bat's loudness usually drops, and its pulse emission rate rises as it approaches its meal.

Step 6: Selection of optimal solution

Every solution is assessed and arranged based on its fitness values at each iteration. The global best solution (gbest) is updated in accordance with the solution that has the highest fitness. This procedure guarantees that the algorithm tracks and maintains the best solution for the size and matching position of DGs.

5.2. *Particle swarm optimization*

Kennedy and Eberhart first presented particle swarm optimization in Ref. [44]. It is a swarm intelligence-based optimization technique that draws inspiration from bird groups' foraging habits. Optimizing a search process by mimicking the behavior of particles in a swarm is the fundamental idea behind PSO. A candidate solution is represented by each particle in the swarm, which navigates the search space by adjusting its position and velocity in response to both its personal experience and the swarm's collective knowledge. In particular, a particle's position relates to the value of a potential solution, whereas its velocity dictates the search's direction and scope. The fitness function is used to evaluate their performance and informs updates to the best location obtained by the swarm as a whole (global best) and the best position found by each particle (personal best) [45]. The particle's position and velocity can be updated using the following formula:

$$v_j^{(i+1)} = \text{k}\left[\begin{array}{c} w * v_j^{(i)} + c_1 rand_1 * (pbest_j - x_j^{(i)} + c_2 rand_2 \\ * \left(gbest_j - x_j^{(i)}\right. \end{array}\right] \tag{45}$$

$$x_j^{(i+1)} = x_j^{(i)} + v_j^{(i+1)};\ j = 1, 2, 3 \ldots\ldots n_s \tag{46}$$

where v_j and x_j are the particle velocity and current position at the generation, w is the factor of inertia weight. Rand is a random number between 0 and 1, and n_s represents the number of swarms. The symbols c_1 and c_2 stand for the acceleration coefficients. The inertia weight formula is generally written as:

$$w = w_{max} - \frac{w_{max} - w_{min}}{i_{max}} * i \tag{47}$$

This approach aids in striking a balance between early iterations of exploration (global search) and later iterations of exploitation (local search). The current iterations are thus indicated by i, while the maximum number of iterations is i_{max}. In every run, the weight of inertia, represented by w_{max} and w_{min}, decreases linearly from 0.9 to 0.4. The stability analysis yields the factor restriction k in PSO, which is very useful when analyzing the convergence behavior of a particle's trajectory over time. Mathematically, k can be expressed as:

$$k = \frac{2}{\left|2 - c - \sqrt{c^2 - 4c}\right|} \text{ where, } c = c_1 + c_2 \text{ and } c < 4 \tag{48}$$

5.2.1. Steps for the PSO algorithm

This section describes how to solve the optimal position and sizing of DG in a grid-connected microgrid using the suggested PSO approach. The steps that follow are described as:

Step 1: Input the microgrid data (line and bus), bus voltage limits, and load demand.
Step 2: Sets the iteration number i = 0 and randomly creates an initial population of particles with random locations and velocities in the solution space.
Step 3: Use Eq. (22) to determine the total loss for each particle if the bus voltage is within the bounds. That particle is not viable otherwise.
Step 4: Each particle updates its personal best (P_{best}) when a lower objective value is achieved, storing the corresponding position.
Step 5: Set the value of the particle linked to the lowest individual best P_{best} of all particles as the current best G_{best}.
Step 6: Update the particle's position and velocity by using Eqs. (26) & (36).
Step 7: Proceed to step 8 if the iteration number exceeds the upper limit. If not, return to step 3 after setting the iteration index, $i = i + 1$.
Step 8: Print out the optimal solution to the target problem. The ideal position comprises the DG's ideal placements and sizes, as well as the matching fitness rating that indicates the least amount of power loss.

5.3. Quantum particle swarm optimization

The authors of Ref. [46] presented QPSO, an improved version of the traditional PSO algorithm that uses concepts from quantum mechanics to improve convergence behavior and global search capabilities. Every particle in QPSO has a quantum state that is defined by a probability density function (PDF), which is usually obtained from a model of a delta potential well. This probability distribution, which is focused around a local attractor, is used to sample the particle's future position. A more balanced exploration–exploitation trade-off is made possible by this attractor, which is described as a weighted mixture of the particle's personal best and the global best locations. The swarm can explore the solution space extensively in the early stages and effectively converge toward the global optimum in the later stages since this coefficient gradually lowers over iterations [47,48]. At every iteration, the particle's position is changed in accordance with Eqs. (49) & (50).

$$x_{p,q}(t+1) = P_{p,q}(t) \pm \xi * \left|mbest_{p,q}(t) - x_{p,q}(t)\right| * In\left(\frac{1}{u}\right) \tag{49}$$

$$P_{p,q}(t) = \left(\varphi * P_{p,q}(t) + (1-\varphi)G_q(t)\right) \tag{50}$$

$$\varphi = \frac{c_1 r_1}{c_1 r_1 + c_2 r_2} \tag{51}$$

In quantum mechanics, the contraction–expansion coefficient, or parameter ξ, is defined as $\xi = 1 - (1.0 - 0.5) * k/G_m$. The contraction–expansion coefficient controls the position update mechanism's search range and rate of convergence. A crucial part in managing the balance between exploration and exploitation during the optimization process is the constant k, which stands for the current iteration count, and G_m, which stands for the maximum number of iterations. In M iterations, every particle with a dimension of D out of N particles converges to its local attractor $P = P_1, P_2, P_3, \ldots, P_D$. The weighting factor, often called a sharing coefficient used to distribute or proportionally allocate quantities between two components or sources, is represented as φ. The acceleration coefficients are c_1 and c_2, the randomly distributed, regularly distributed integers within [0, 1] are r_1, r_2 and u, respectively. The personal best and global best positions of the p^{th} particle in the q^{th} iteration is indicated by $P_{p,q}$ and G_q. For each iteration, the average of the individual best locations $mBest_{p,q}(t)$ is needed to update the lagged particles into the population.

$$mBest_{p,q}(t) = \frac{1}{N}\sum_{p=0,q=1}^{N,M} P_{p,q}(t)$$
$$\left(\frac{1}{N}\sum_{p=0}^{N} P_{p,1}(t), \frac{1}{N}\sum_{p=0}^{N} P_{p,2}(t), \ldots, \frac{1}{N}\sum_{p=0}^{N} P_{p,D}(t)\right) \tag{52}$$
$$\text{Provided}, (1 \le p \le N)\text{and}(1 \le q \le M)$$

5.3.1. Steps for the QPSO algorithm

This section covered the procedures for determining the ideal location and size of DG in a grid-connected microgrid using the suggested QPSO technique. The subsequent actions are explained as follows:

Step 1: Input the microgrid system data, such as load demand, DG limits, acceptable bus voltage limits, line and bus specifications.
Step 2: Create an initial population of particles indicating potential DG sites and sizes at random points in the solution space. Set $t = t + 1$ as the initial value for the iteration counter.
Step 3: Examine each particle's viability by confirming that all bus voltages fall within the permitted ranges.
Step 4: Determine the mean optimal position '$mBest_{p,q}(t) = \frac{1}{Gm}\sum_{p=1}^{Gm} P_{p,q}(t)$' and select an appropriate contraction-expansion ξ value.
Step 5: Use Eq. (22) to calculate the overall power loss if the voltage restrictions are met. If not, the particle is considered unfeasible.
Step 6: Compare each particle's personal best value $P_{p,q}$ with its current objective function value of $x_{p,q}(t+1)$. Update $P_{p,q}$ and record the appropriate particle position if the current value $x_{p,q}$ is less than $P_{p,q}$.
Step 7: Select the particle with the minimum personal best $P_{p,q}$ value among all particles and assign it as the global best position G_q.
Step 8: From Eqs. (26) & (36), the particle locations are updated according to the quantum-behaved position.
Step 9: Go to step 10 if the iteration number exceeds the maximum predetermined limit; if not, increase the iteration counter $t = t + 1$ and go back to step 5.
Step 10: Print out the optimal solution to the target problem. The ideal position comprises the DG's ideal placements and sizes, as well

as the matching fitness rating that indicates the least amount of power loss.

5.4. Pareto concept for multi-objective approach

Pareto optimality, which states that no objective can be enhanced without degrading at least one other objective, takes the place of the conventional concept of optimality in a minimization framework. Instead of producing a single optimum, an algorithm usually produces a group of optimal trade-off solutions inside the Pareto framework of multi-objective optimization. A feasible solution that is not dominated by any other possible option is called a Pareto-optimal solution [49]. Let $X^* \in \mathscr{F}$ represent a potential solution within the feasible set $\mathscr{F}$. The solution X^* is said to be Pareto optimal if another solution does not exist $X \in \mathscr{F}$ such that:

$$F(X) = [f_1(X),\ f_2(X)....f_O(X)] \tag{53}$$

$$f_p(X) \le f_p(X^*) \text{ for all } p = 1,\ 2, ..., O \tag{54}$$

$$f_q(X) < f_q(X^*) \text{ for at least one } q \in \{1,\ 2, ..., O\} \tag{55}$$

where, X is a feasible solution, and O denotes the number of objective functions. A solution X is said to dominate another solution X^* for a minimization problem, if it satisfies both conditions from Eq. (54) & (55), respectively.

5.5. Best-compromise-solution method

This research uses a fuzzy decision-making strategy to find the optimal compromise solution utilizing a Pareto-based multi-objective optimization framework. A decision-making method is needed to choose a single solution that offers a balanced trade-off among the competing objective functions after the Pareto-optimal set of non-dominated alternatives has been generated. In order to achieve this, each objective function is evaluated and normalized using a fuzzy membership function [50]. The membership value $\left(\mu_x^f(X)\right)$, that corresponds to the x-th objective function is defined as follows:

$$\mu_x^f(X) = \begin{cases} \dfrac{f_x^{max} - f_x(X)}{f_x^{max} - f_x^{min}}; & f_x^{min} \le f_x(X) \le f_x^{max} \\ 0; & f_x(X) \ge f_x^{max} \\ 1; & f_x(X) \le f_x^{min} \end{cases} \tag{56}$$

The membership function is a continuous, strictly monotonically decreasing function that has a range of 0 to 1. The Pareto-optimal solutions for each objective function $f_x(X)$ are used to calculate the lower and upper limits, f_x^{min} and upper f_x^{max}. The decision-maker chooses the best compromise solution after getting all Pareto-optimal choices based on particular preferences. The following is how the best compromised solution is chosen:

$$N_\mu(l) = \frac{\sum_{i=1}^{n} \omega_i \times \mu_{li}}{\sum_{l=1}^{m} \sum_{i=1}^{n} \omega_i \times \mu_{li}} \tag{57}$$

where n is the number of objective functions, m is the number of non-dominated solutions, and ω_i is the weight factor connected to the i^{th}objective function. The fuzzy membership value of the i^{th} objective for the i^{th} solution is represented by the number μ_{li}. Suppose that $i = 0, 1, 2, 3$…and that the weighting factor is set to 0.25.

6. Simulation results and discussion

The suggested optimization algorithm results for the DG placement problem are displayed in this section. In this research, Fig. 2 displays the measured distribution system data of a modified IEEE 33-bus test system. The system's simplicity results in faster solutions. Nevertheless, the systems limit optimal locations. Although they cannot provide 100% certainty, the suggested algorithms effectively handle the system's problems and provide quick fixes. The suggested optimization strategy is implemented using MATLAB R2021b version 9.10.0.1577079 program for result analysis and visualization. The experimental simulation was conducted using a Dell Core i5-latitude E7270 CPU running at 2.50 GHz and 8 GB of RAM. Limiting the computation time per scheduling instance to 10 min enables near real-time optimization. (N), which represents the swarm size, is set to 50. With each run, w_{min} decreases linearly to 0.4 while w_{max}, the weight of inertia, is set to 0.9. The maximum number of iterations ($iter_{max}$) is set to 0 to 200. Parameter values of 1.5 and 2.0 are assigned to the social acceleration coefficient c_1 and cognitive acceleration coefficient c_2, respectively. The contraction-expansion coefficient (ξ) on the other hand, is fixed at 0.5 and is essential for controlling the particle search behavior.

6.1. DG source and bus location

As stated in Section 2, the system included an FC, WT, and solar PV system. Figs. 7, 8, and 9 depict the power produced by each DG source, respectively. The available solar irradiation determined how much solar PV power was produced. The sun irradiance power is absent from 0 to 5 h and from 19 to 24 h, as shown in Fig. 7. The solar power generated peaked between 12 and 14 h later. In Fig. 8, the wind profile is dynamic and changes over time. The wind turbine generated peaked between 20 and 22 h and later fell between 23 and 24 h. Fig. 9 illustrates how the fuel cell output power remained consistent during the course of the 24 h under consideration. As a result, the overall amount of DG power produced is dynamic and peaks at midday. Fig. 10 shows the entire DG power generation in Eq. (13). Depending on how generation and load demand are balanced, the simulated power exchange at the point of common coupling (PCC) over 24 h displays bidirectional behavior, suggesting both grid import and export. When the demand for DG power generation is unable to be met by the grid. Positive numbers show grid support when local resources are insufficient, and negative values show surplus power generated fed back to the grid. Fig. 11 shows the power across the point of common coupling, or the point where the grid connects to the rest of the system. Consequently, the bus location coefficients (BLCs) were chosen as the criterion for determining the initial network sites for DG. Based on the real BLC computation model, usually derived from loss sensitivity analysis. These BLCs were calculated using the load profile as shown in Fig. 12, at five different load participation levels: 20%, 40%, 60%, 80%, and 100% of the rated power. According to the load profile, the lower load levels result in somewhat greater BLC values. Conversely, the BLC values are lowest at higher load levels.

6.2. Optimal sizing and location of DGs using PSO

Different DG configurations are compared to assess the effect of DG placement on active power losses throughout the 33-bus distribution network. In this research, voltage limitations of 0.95 and 1.05 are considered. The simulation parameter values while using PSO are shown in Table 3. Based on the number of DGs that are ideally positioned and scaled in the system network, four case studies are taken into consideration. Consequently, there are one to four DGs.

- *Case 1:* In the distribution network, one DG is positioned and sized optimally.
- *Case 2:* In the distribution network, two DGs are positioned and sized optimally.
- *Case 3:* In the distribution network, three DGs are positioned and sized optimally.
- *Case 4:* In the test bus system, four DGs are positioned and sized optimally.

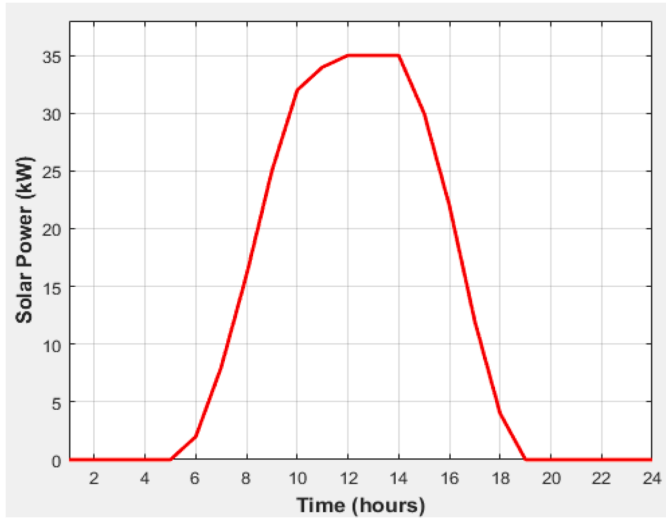

Fig. 7. Power obtained from solar PV.

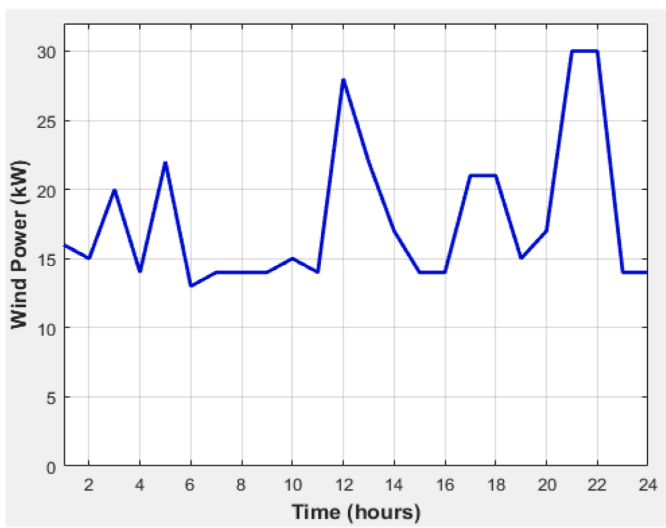

Fig. 8. Power obtained from wind.

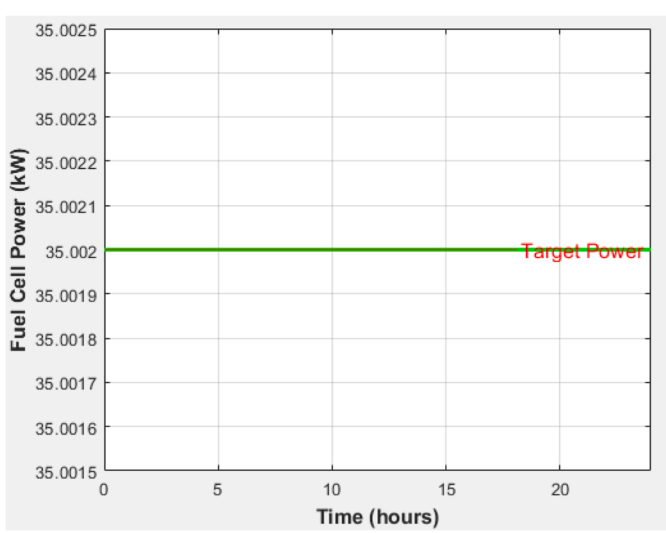

Fig. 9. Power obtained from the fuel cell.

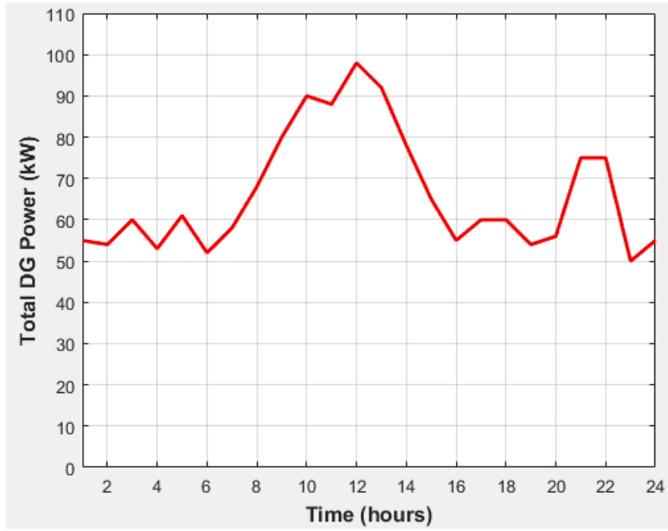

Fig. 10. Total power obtained from DG.

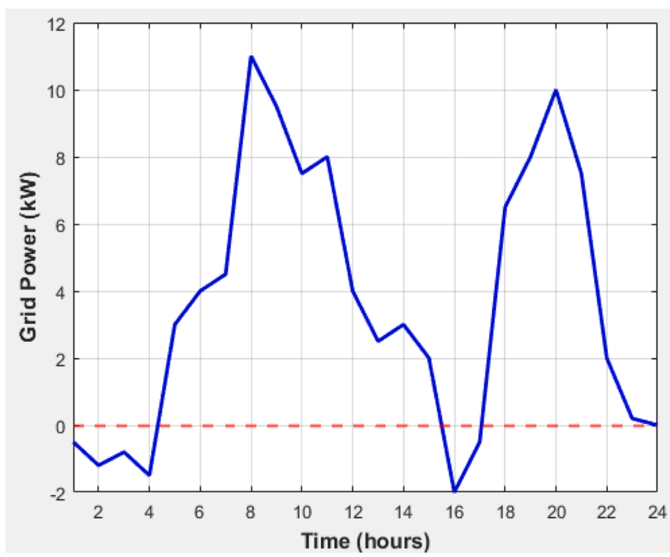

Fig. 11. Power exchange across PCC.

The Fig. 13 compares active power losses across the 33-bus distribution network with DGs and without DGs. In the simulation result, the power loss decreases from 202.67 *kW* to 114.89 *kW*, 86.65 *kW*, 72.42 *kW*, and 66.40 *kW* in the base case, DG-1, DG-2, DG-3, and DG-4, respectively. This yields a percentage reduction of 43.32% over DG-1, 57.27% over DG-2, 64.26% over DG-3, and 67.24% over DG-4. Reactive power loss decreases from 135.14 *kVAr* to 73.90 *kVAr*, 58.68 *kVAr*, 49.81 *kVAr*, and 45.39 *kVAr* of the base case, DG-1, DG-2, DG-3, and DG-4, respectively. As DG units are positioned optimally, reactive power losses drop proportionately with active power losses, indicating better reactive power compensation and decreased network current flow. Fig. 14 shows how the voltage profile of the 33-bus network is much improved over the base scenario when DG units are positioned optimally using PSO. In the base case, there is a noticeable voltage drop that begins at bus 22 and drops to 0.910 *p.u.* While DG-1 at bus 11 raises the voltage to 0.920 *p.u.*, DG-2 and DG-3 increases the voltages to 0.921 *p.u.* and 0.928 *p.u.* In DG-4, buses 7, 14, 25, and 31 obtain the most uniform profile by maintaining all voltages between 0.928 *p.u.* and 0.930 *p.u.*, hence minimizing violations. The Table 4 shows that when the number of DGs rises, both active and reactive power losses consistently decrease. The integration of a single DG reduces losses significantly as compared to the base situation without DGs, and the deployment of many DGs produces increasingly larger gains. In particular, reactive losses drop from 135.01 *kVAr* to 45.39 *kVAr*, and active power losses drop from 202.67 *kW* to 66.40 *kW* These findings demonstrate that a greater number of DGs positioned appropriately improves network performance and loss minimization.

6.3. Optimal sizing and location of DGs using BAT

In this research, DGs are divided into four groups based on their capacity to provide both active and reactive power. The bat algorithm parameters taken into account during the simulation are loudness (A) in the range [2, 0], frequency (f) in the range [0, 2], and pulse rate (r) in the range [0, 1]. The BAT parameter values used for the best DG placement and size in the modified IEEE 33-bus distribution network are summarized in Table 5. The active power losses over the 33-bus distribution network in the base case and different DG integration scenarios from DG-1 to DG-4, optimized using the bat algorithm, are shown in Fig. 15. In the simulation results, system losses significantly decrease as the

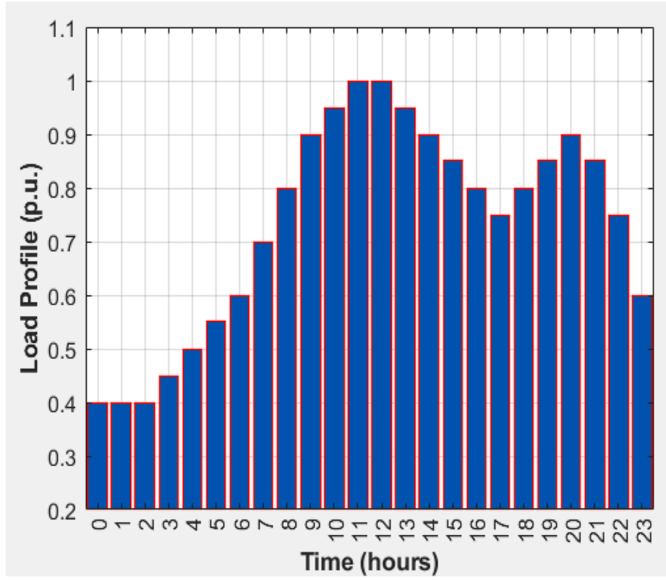

Fig. 12. Schedule of DG load profile.

Table 3
Simulation parameters of PSO for all DGs.

Parameter	Values
Population size (N)	50
Maximum iterations ($iter_{max}$)	200
Minimum weight of inertia (ω_{min})	0.4
Maximum weight of inertia (ω_{max})	0.9
Social acceleration coefficient (c_1)	1.5
Cognitive acceleration coefficient (c_2)	2.0

number of DG units positioned optimally rises.

The base case's total active power loss of 202.67 kW drops to 97.73 kW, 88.01 kW, 67.75 kW, and 57.61 kW, respectively. In comparison to the base case, the percentage reductions are 51.78%, 56.57%, 66.57%, and 71.57% for DG-1, DG-2, DG-3, and DG-4. In a similar vein, the reactive power loss decreases from 135.14 $kVAr$ to 66.17 $kVAr$, 60.31 $kVAr$, 45.62 $kVAr$, and 38.50 $kVAr$ When DG units are positioned optimally, reactive power losses drop proportionately with active power losses, indicating better reactive power compensation and decreased network current flow. Fig. 16 shows how the voltage profile of the 33-bus network is greatly enhanced by BAT-based optimized DG placement. From bus 27 onward, the basic case shows significant voltage loss, falling to 0.910 $p.u.$ A DG-1 installed at bus 33 results in a 0.924 $p.u.$, localized improvement. The tail-end is still weak at 0.920 $p.u.$, even though DG-2 at buses 7 and 15 increases the voltages. Support is further extended at buses 8, 17, and 31 in DG-3, increasing voltages at buses 31 and 33 to 0.924 $p.u.$ and 0.928 $p.u.$, respectively. By raising the minimum voltage to 0.934 $p.u.$ and guaranteeing that all buses stay well within allowable bounds, the ideal configuration—DG-4 at buses 5, 12, and 29—achieves the most consistent voltage profile.

6.4. Optimal sizing and location of DGs using QPSO

Four different DG configurations are compared using QPSO to assess the effect of DG placement on active power losses throughout the 33-bus distribution network. The voltage limitations used in this investigation are 0.95 and 1.05. Table 6 shows the simulation parameter values while using QPSO. When choosing the contraction-expansion coefficient ξ, social acceleration coefficient (c_1), and cognitive acceleration coefficient (c_2), it is important to consider the following factors into account.

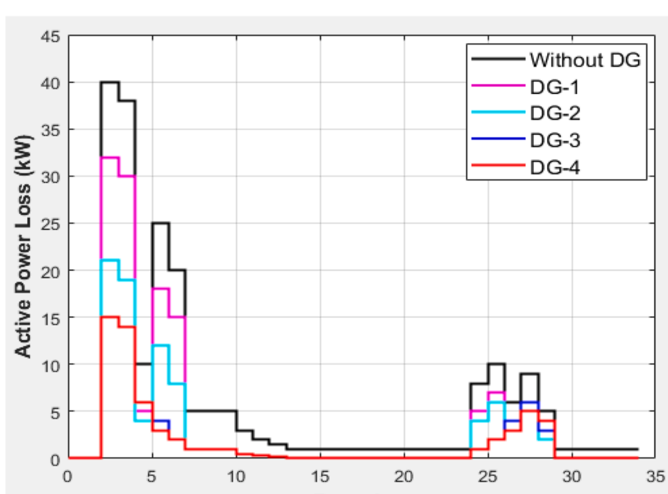

Fig. 13. Power losses for all DGs using PSO.

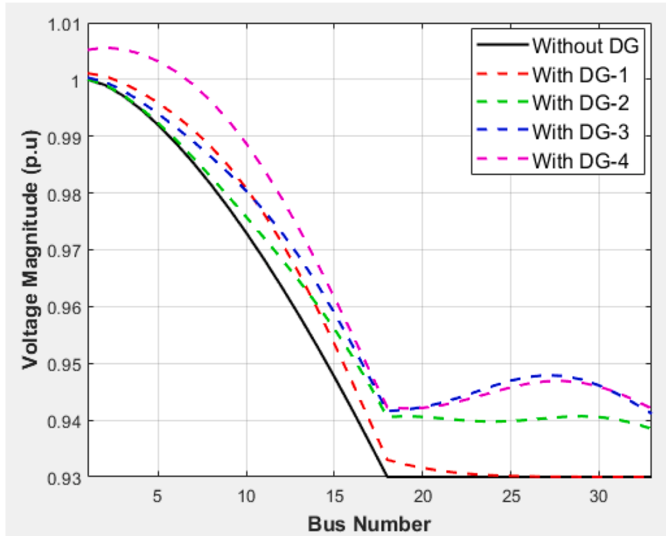

Fig. 14. Voltage magnitude for all DGs using PSO.

Table 4
Optimal sizing and location of DGs obtained by PSO.

Cases	Optimal placement of DG (bus)	Optimal size of DG (*MW*)	Optimal size of DG (*kVAr*)	Active loss (*kW*)	Reactive loss (*kVAr*)	Voltage magnitude (*p.u.*)	Efficiency (%)
Without DG	-	-	-	202.67	135.01	0.910	-
With DG-1	11	1.000	0.484	114.89	73.90	0.920	43.32
With DG-2	30	1.000	0.484				57.27
	18	0.893	0.432	86.65	58.68	0.921	
With DG-3	30	1.000	0.484				64.26
	25	0.837	0.405	72.42	49.81	0.928	
	14	0.791	0.383				
With DG-4	7	0.869	0.421				67.24
	14	0.582	0.282	66.40	45.39	0.930	
	31	0.710	0.344				
	25	0.719	0.348				

Table 5
Simulation parameters of BAT for all DGs.

Parameter	Values
Maximum iterations	200
Population size	20
Loudness	0.9
Frequency	0.9

- Particles are drawn more to their own optimal position if $c_1 > c_2$, which increases self-exploration but leads to an excessive number of scattering particles.
- On the other hand, when $c_2 > c_1$, particles are strongly attracted toward the global best position, it increases the risk of premature convergence to local optima.
- When $c_1 = c_2$, particles are equally influenced by both personal best and global best positions, resulting in a balanced exploration–exploitation behavior around the search space centroid.
- The contraction–expansion coefficient ξ plays a crucial role in controlling the convergence behavior of the swarm, where bigger values enhance global exploration and smaller values boost local exploitation and fine-tuning of the optimal solution.

The comparison of active power losses across the 33-bus distribution network, optimized using the QPSO, between the base case (without DG) and different DG integration scenarios is shown in Fig. 17. The simulation results show that the number of optimally placed DG units significantly reduces system losses. In particular, the base case's total active power loss of 202.67 *kW* drops to 96.85 *kW*, 87.30 *kW*, 66.40 *kW*, and 52.15 *kW* In comparison to the base scenario, the percentage loss reduction are 52.21%, 56.92%, 67.24%, and 74.27% for DG-1, DG-2, DG-3, and DG-4, respectively. In a similar vein, the reactive power loss decreases from 135.14 kVAr to 64.90 *kVAr*, 59.45 *kVAr*, 44.20 *kVAr*, and 36.10 *kVAr* in the base case, DG-1, DG-2, DG-3, and DG-4, respectively. Consequently, when the number of strategically positioned DG units rises, reactive power losses fall proportionately with active power losses, providing better reactive power compensation, lower line current, and increased distribution network efficiency under QPSO-based planning. Fig. 18 shows how the voltage profile of the 33-bus distribution network is greatly enhanced by QPSO-based optimal DG placement. Due to inadequate voltage regulation, the basic case shows significant voltage degradation, falling to 0.930 *p.u.* from bus 22. The voltage at bus 30 increased to about 0.933 *p.u.* Due to the integration of DG-1, the effect was only seen at the tail end. Buses 14 and 30 now have DG-2 installed, which raises voltage levels. Deployed on buses 6, 18, and 31, DG-3 increases voltage support to 0.935 *p.u.* and 0.938 *p.u.* at buses 31 and 33, respectively. The most efficient design, DG-4, raises the minimum bus voltage to 0.949 *p.u.*, improving system stability and power quality, and delivering the flattest and highest voltage profile throughout the network with units ideally positioned at buses 7, 14, 25, and 30.

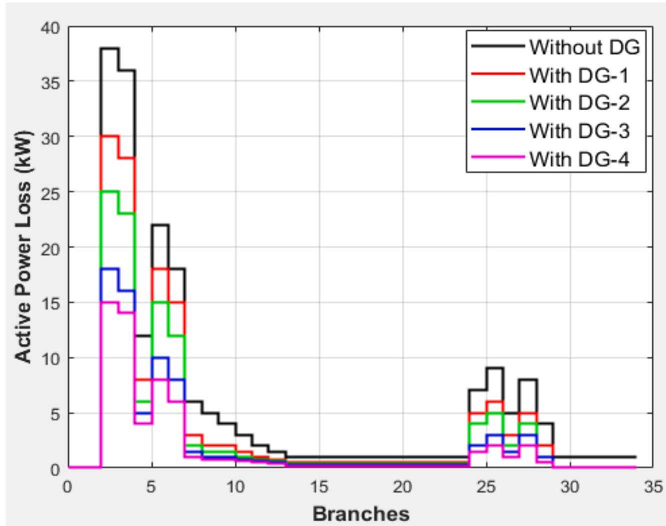

Fig. 15. Power losses for all DGs using the BAT algorithm.

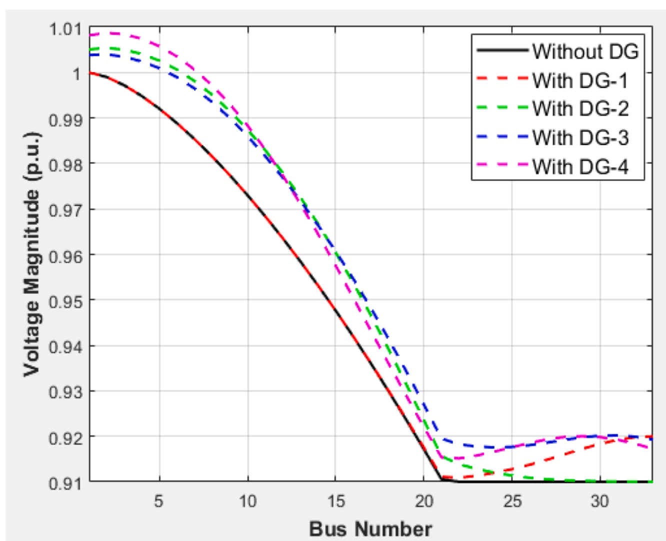

Fig. 16. Voltage magnitude for all DGs using the BAT algorithm.

Table 6
Simulation parameters of QPSO for all DGs.

Parameter	Values
Number of particles (N)	50
Maximum number of iterations ($iter_{max}$)	200
Contraction–expansion coefficient (ξ)	0.5
Social acceleration coefficient (c_1),	1.5
Cognitive acceleration coefficient (c_2)	2.0

6.5. Convergence characteristics with computational efficiency of active power losses

The convergence plot with computational efficiency of active power for all DGs using PSO is shown in Fig. 19. The convergence curves show that the PSO algorithm effectively reduces active power loss as the number of iterations increases. The base case without DG remains constant at a high loss of 202.67 kW since no optimization is applied. In contrast, all DG cases exhibit a rapid decrease in losses during the initial iterations, followed by gradual stabilization. Among the configurations, DG-4 achieves the lowest final loss of 66.40 kW, indicating the best performance, while DG-1 of 114.89 kW, has the highest loss among the DG cases. This confirms that increasing the number of DG units improves loss minimization. The computational time increases slightly from DG-1 at 0.101 sec to DG-4 at 0.265 sec, reflecting the higher complexity and search space associated with multiple DG placements. Despite this, all cases converge within a short time, demonstrating the efficiency of the PSO algorithm. Consequently, after 50 trials of the simulation, this study selects the worst, average, and best results from feasible solutions. Table 7 presents the statistical performance analysis after 50 trials using PSO. The statistical analysis demonstrates consistent convergence performance. The DG-4 configuration yields the lowest active power loss and highest voltage profile, with minimal deviation between best and worst cases, indicating robustness and stability of the optimization process. In contrast, the base case (without DG) shows no variability due to the absence of optimization.

In a similar vein, the convergence plot with computational efficiency of active power for all DGs using the BAT algorithm is shown in Fig. 20. The base case without DG remains constant at a high loss of 202.67 kW since no optimization is applied. In contrast, all DG cases exhibit a rapid decrease in losses during the early iterations, followed by a smooth and stable convergence. Among the configurations, DG-4 achieves the lowest

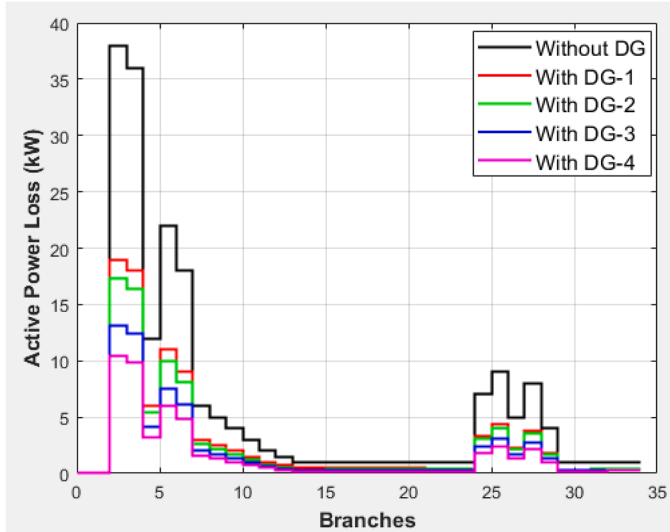

Fig. 17. Power losses for all DGs using QPSO.

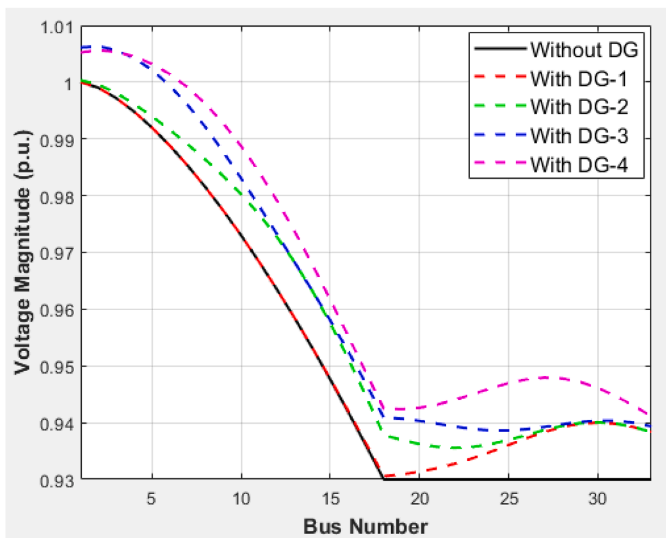

Fig. 18. Voltage magnitude for all DGs using QPSO.

final loss of 57.61 kW, indicating the best performance, while DG-1 of 97.73 kW, records the highest loss among the DG cases. This demonstrates that increasing the number of DG units significantly enhances loss minimization. The computational time increases slightly from DG-1 at 0.133 *sec* to DG-4 at 0.282 *sec*, due to the increased complexity and higher-dimensional search space associated with multiple DG placements. However, all cases converge within a short time, confirming the efficiency of the BAT algorithm compared to PSO. Consequently, Table 8 presents the statistical performance analysis after 50 trials using the BAT algorithm. The statistical analysis demonstrates a consistent and stable convergence behavior across all test cases. The results indicate that the BAT algorithm maintains reliable optimization performance with minimal variation between best, average, and worst outcomes, confirming its robustness in solving the DG allocation problem in the IEEE 33-bus system. Among all configurations, the DG-4 case achieves the most optimal performance, recording the lowest active power loss and the highest voltage magnitude of 0.934 $p.u.$ The small deviation between the best and worst solutions further highlights the stability and reliability of the BAT optimization process, indicating strong convergence characteristics and low sensitivity to random initialization.

The convergence characteristics show that the QPSO algorithm effectively reduces active power loss as the number of iterations increases in Fig. 21. Among the configurations, DG-4 achieves the lowest final loss of 52.15 kW, indicating the best performance, while DG-1 of 96.85 kW, records the highest loss among the DG cases. This demonstrates that increasing the number of DG units significantly enhances loss minimization. The computational time increases slightly from DG-1 at 0.113 *sec* to DG-4 at 0.285 *sec*, due to the increased complexity and higher-dimensional search space associated with multiple DG placements. However, all cases converge within a short time, confirming the efficiency of the QPSO. The QPSO algorithm demonstrates superior convergence performance compared to PSO and BAT. It achieves the lowest active power loss, along with an improved voltage magnitude of 0.949 pu. The convergence curves indicate faster and smoother reduction in losses, highlighting the strong global search capability of QPSO. In Table 9, the statistical performance analysis after 50 trials using QPSO for all DG cases is presented. The statistical analysis demonstrates consistent convergence performance. The DG-4 configuration yields the lowest active power loss and highest voltage profile, with minimal deviation between best and worst cases, indicating robustness and stability

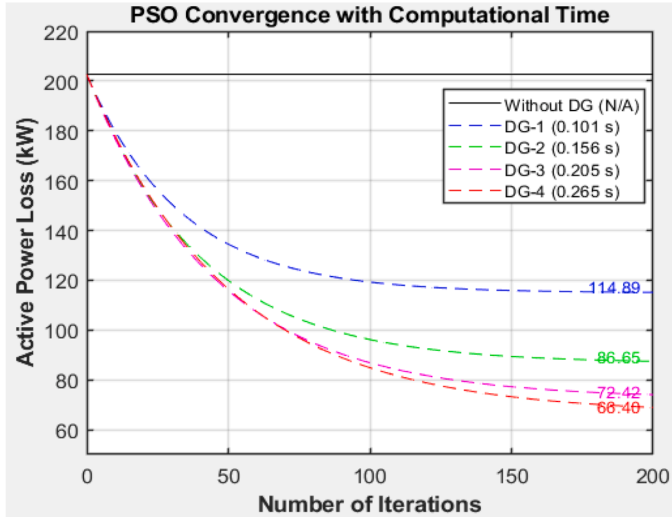

Fig. 19. Convergence of power loss for all DGs using PSO.

Table 7
Statistical performance analysis for all DGs using PSO (worst, best, average, standard deviation results after 50 trials).

Objective	Cases	Average	Best	Worst	STD (σ)
	Without DG	202.67	202.67	202.67	0.000
	DG-1	116.20	114.89	118.75	0.965
P_1 (kW)	DG-2	88.10	86.65	90.30	0.913
	DG-3	73.95	72.42	76.10	0.920
	DG-4	68.05	66.40	70.25	0.963
	Without DG	0.910	0.910	0.910	0.0000
	DG-1	0.918	0.920	0.915	0.00125
V_1 ($p.u$)	DG-2	0.919	0.921	0.916	0.00125
	DG-3	0.926	0.928	0.923	0.00125
	DG-4	0.928	0.930	0.925	0.00125

of the optimization process. In contrast, the base case shows no variability due to the absence of optimization.

A comparison of several optimization strategies used to reduce loss in the IEEE 33-bus distribution system is shown in Table 10. The suggested optimization techniques are compared to current methodologies based on important performance parameters, such as minimum bus voltage, active power loss, percentage loss reduction, and ideal DG location and size. It is clear from the data that the suggested QPSO approach improves the voltage profile and reduces losses more effectively throughout the network. In comparison to Multi-Objective Particle Swarm Optimization (MOPSO) [51], Comprehensive Learning Particle Swarm Optimization (CLPSO) [52], Multileader Particle Swarm Optimization (MLPSO) [53], Constriction Coefficient Particle Swarm Optimization (CCPSO) [54], and the other suggested algorithms, QPSO produces the lowest power loss and the highest percentage loss

Table 8
Statistical performance analysis for all DGs using BAT (worst, best, average, standard deviation results after 50 trials).

Objective	Cases	Average	Best	Worst	STD (σ)
	Without DG	202.67	202.67	202.67	0.000
	DG-1	97.73	96.85	99.10	0.563
P_2 (kW)	DG-2	88.01	87.30	89.25	0.488
	DG-3	67.75	66.40	69.10	0.675
	DG-4	57.61	52.15	59.80	1.913
	Without DG	0.910	0.910	0.910	0.0000
	DG-1	0.924	0.926	0.921	0.00125
V_2 ($p.u$)	DG-2	0.920	0.922	0.918	0.00100
	DG-3	0.928	0.930	0.925	0.00125
	DG-4	0.934	0.936	0.931	0.00125

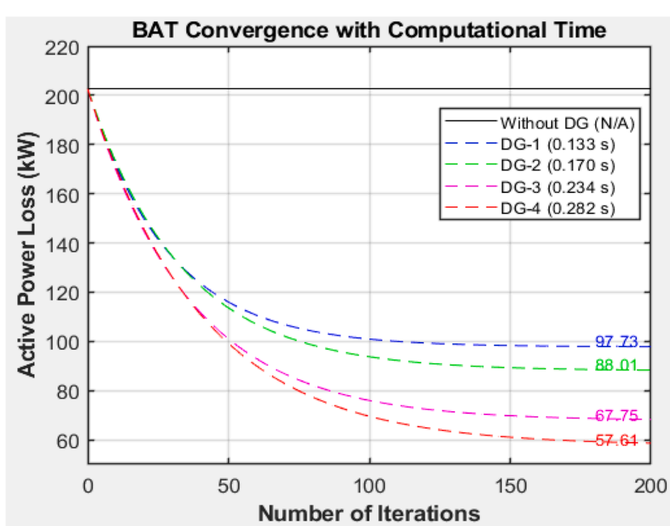

Fig. 20. Convergence of power loss for all DGs using BAT.

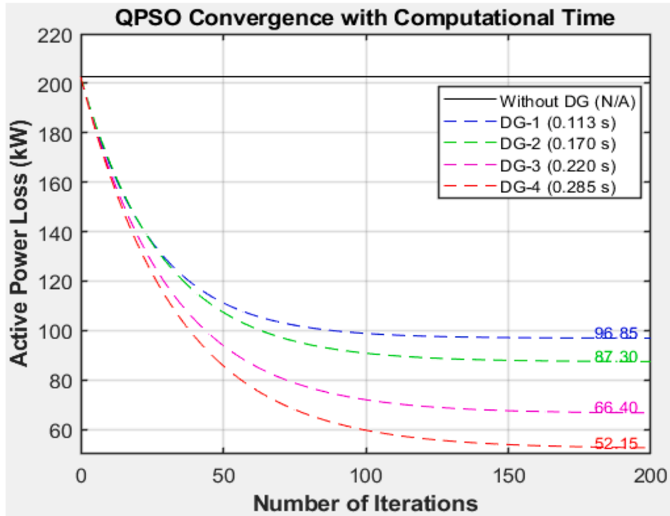

Fig. 21. Convergence of power loss for all DGs using QPSO.

Table 9
Statistical performance analysis for all DGs using QPSO (worst, best, average, and standard deviation results after 50 trials).

Objective	Cases	Average	Best	Worst	STD (σ)
	Without DG	202.67	202.67	202.67	0.000
	DG-1	97.10	96.85	98.20	0.338
P_3 (kW)	DG-2	88.05	87.30	89.40	0.525
	DG-3	67.20	66.40	68.90	0.625
	DG-4	53.85	52.15	55.10	0.738
	Without DG	0.930	0.930	0.930	0.000
	DG-1	0.933	0.935	0.931	0.0010
V_3 ($p.u$)	DG-2	0.935	0.936	0.933	0.0008
	DG-3	0.938	0.939	0.936	0.0008
	DG-4	0.949	0.951	0.947	0.0010

reduction with the deployment of four DG units, indicating its efficacy for the best DG sizing and placement in distribution networks.

6.6. *Pareto framework of multi-objective optimizations*

The Pareto fronts produced by the multi-objective optimization algorithms are presented in this section. By minimizing the multi-objective functions specified in Eqs. (27) to (35), while taking into account all DG performance measures, such as generation cost, voltage deviation, power losses, and emissions, the Pareto optimal solutions are obtained. In this research, two (2) out of four (4) Pareto fronts are presented. Pareto front comparison of multi-objective optimization algorithms illustrating the trade-off between power losses and voltage deviation is depicted in Fig. 22. From the simulation, the solutions of the QPSO algorithm dominate the solutions obtained by PSO and BAT. When compared to PSO and BAT, QPSO achieves better trade-off solutions with improved voltage deviation at lower power losses. QPSO achieves a voltage deviation of around 2.36 $p.u.$ at about 52 kW power loss, while PSO and BAT need about 66 kW and 87 kW, respectively, to achieve similar deviation levels. Due to the use of quantum-enhanced metaheuristics for multi-objective planning across distribution networks, the QPSO algorithm has a greater diversity than alternative

Table 10
Comparative results of the optimal sizing and location of DG across the standard IEEE 33-bus system.

Optimization	DG No.	Optimal location (bus)	Optimal size (kW)	Power loss (kW)	Loss reduction (%)	Minimum voltage ($p.u.$)
MOPSO [51]	DG-1	6	1.42	102.33	51.27	-
	DG-2	11	0.96	82.99	60.49	-
	DG-3	29	1.08	73.63	64.94	0.929
CLPSO [52]	DG-1	6	1.43	102.13	51.40	-
	DG-2	30	1.10	81.72	61.10	-
	DG-3	11	0.93	70.30	66.54	0.932
MLPSO [53]	DG-1	6	1.42	102.12	51.40	-
	DG-2	30	1.15	81.62	61.15	-
	DG-3	11	0.76	68.46	67.40	0.936
CCPSO [54]	DG-1	8	0.33	163.64	19.47	0.922
	DG-2	30	1.21	90.17	55.62	0.934
	DG-3	19	0.51	78.27	61.48	0.939
Proposed PSO	DG-1	11	1.000	114.89	43.32	0.920
	DG-2	30	1.000	86.65	57.27	0.921
	DG-3	25	0.837	72.42	64.26	0.928
	DG-4	7	0.869	66.40	67.24	0.930
Proposed BAT	DG-1	33	1.492	97.73	51.78	0.924
	DG-2	15	0.484	88.01	56.57	0.920
	DG-3	8	0.374	67.75	66.57	0.928
	DG-4	29	0.478	57.61	71.57	0.934
Proposed QPSO	DG-1	30	1.520	96.85	52.21	0.933
	DG-2	14	0.412	87.30	56.92	0.935
	DG-3	6	0.381	66.40	67.24	0.938
	DG-4	25	0.489	52.15	74.27	0.949

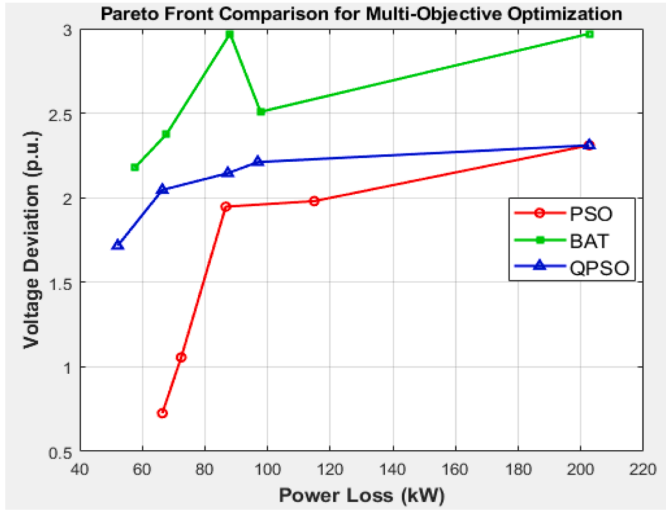

Fig. 22. Voltage deviation–power loss trade-off.

methods. Using multi-objective optimizations, Fig. 23 shows the Pareto front between total emission and generating cost. From the simulation, the solutions of the QPSO algorithm dominate the solutions obtained by PSO and BAT. When compared to PSO and BAT, QPSO achieves better trade-off solutions with total emission reduction at a lower generating cost. With an emission of about 110 *kg*, QPSO achieves a cost of about \$6640, while PSO needs about \$6660, and BAT costs around \$6655. The Pareto analysis demonstrates that QPSO provides the most effective and balanced DG integration method, providing the best balance between total emission and generation cost. Because they achieve lower emissions at lower operating costs, QPSO solutions dominate the Pareto front.

6.7. Best compromise solution using fuzzy approach

This section presents a fuzzy decision-making method for optimizing three objective functions at the same time. Refer to Eq. (56), fuzzy membership functions are used to evaluate and normalize each objective function. Based on operational priorities, the distribution system decision-maker allocates weight factors to the objective functions. The optimal compromise solution, marked by the black star in Fig. 24, represents the best trade-off among power loss, emission, and cost objectives. The QPSO algorithm achieves minimum values of approximately 52 *kW* power loss, 5 *kg* emissions, and \$5 operating cost through the optimal placement of DG-4 units at buses 7, 14, 25, and 30. This configuration also maintains a minimum voltage magnitude of 0.949 *p.u.* and improves the overall system efficiency to 74.27%. In a similar vein, Fig. 25 shows the best compromise solution, represented by the black star, at the lower corner of the feasible region. It has a cost of around \$6.5, emissions of about 50 *kg*, and a voltage deviation of about 0.8 *p.u.*, reflecting the optimum trade-off between all objectives. With DG-4 units strategically positioned at buses 7, 14, 25, and 30, this solution matches the QPSO-based design that delivers the highest minimum bus voltage of 0.949 *p.u.*, the lowest active power loss of 52.15 *kW*, and the highest loss reduction efficiency of 74.27%

7. Conclusion

This work has demonstrated the ideal placement and size of DGs in grid-connected microgrids for loss reduction and voltage profile improvement using PSO, BAT, and QPSO optimization approaches. Deploying optimization strategies is important for handling large-scale, complicated energy management issues, making decisions in real time, adapting to changing conditions, minimizing losses, and improving

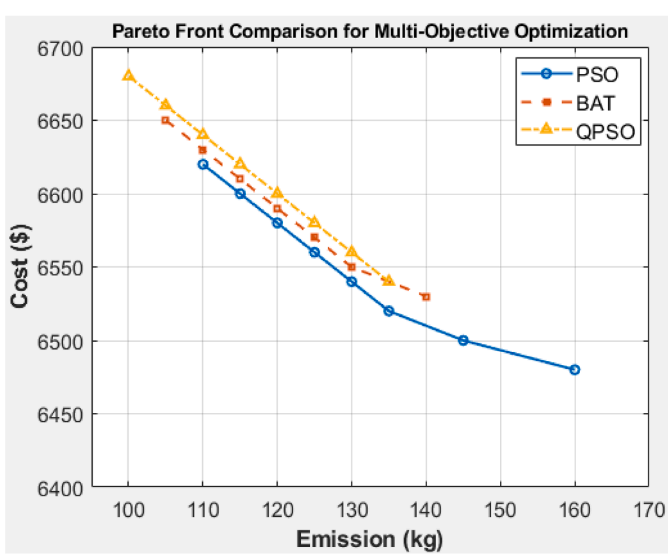

Fig. 23. Generation cost–emission trade-off.

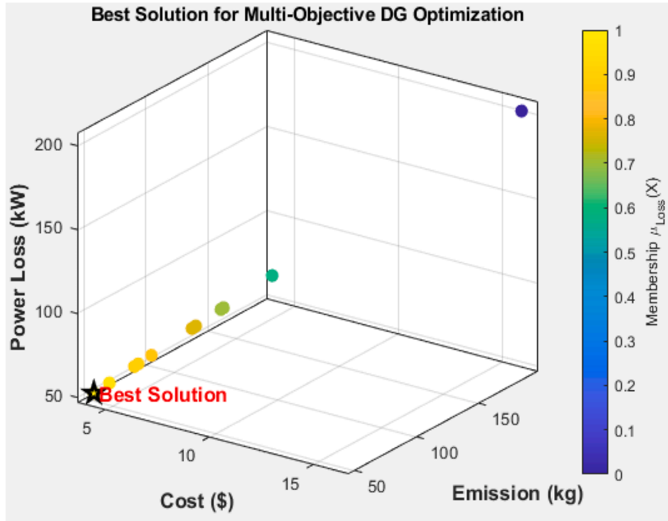

Fig. 24. Pareto-optimal solution of three objective functions: active power loss, emissions, and cost.

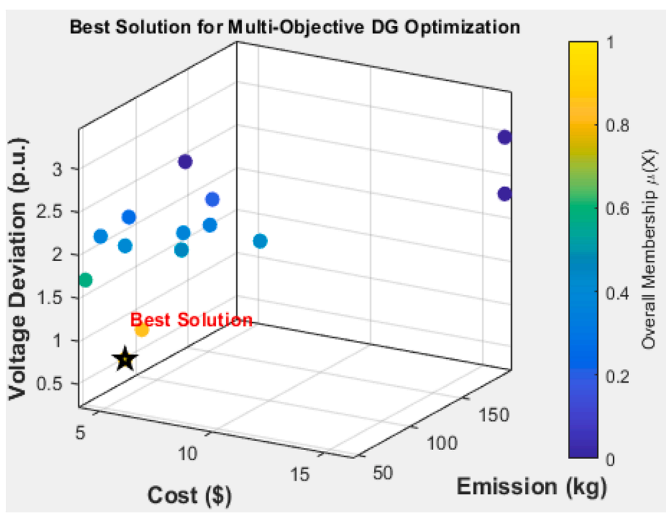

Fig. 25. Pareto-optimal solution of three objective functions: voltage deviation, cost, and emissions.

system performance. The four DGs' objective functions have been optimized using the Pareto-fronts-based optimization framework, which applies a fuzzy decision-making tool to get the optimum compromise solution. Based on how many DGs are ideally positioned and scaled in the system network, four case studies are taken into consideration in the research. The effectiveness of the suggested methods was confirmed using a modified IEEE 33-bus test system, which is a well-known distribution network benchmark. The simulation results demonstrate that the suggested method can reduce the test bus system's generating costs, power losses, voltage variations, and emissions. As a result, in comparison to other optimization techniques already in use, the methods tackling optimal DG placement difficulties achieved loss reductions ranging from 43.32% to 67.24% of PSO, 51.78% to 71.57% of BAT, and 52.21% to 74.27% of QPSO. Similarly, the techniques enhanced the voltage profile ranging from 0.920 pu. to 0.930 *p.u.* of PSO, 0.924 *p.u.* to 0.934 *p.u.* of BAT, and 0.933 *p.u.* to 0.949 *p.u.* Throughout the test system network, the DGs' voltage profiles improved. The primary benefits of the suggested algorithm are its capacity to produce many Pareto optimal solutions, which aid the decision-maker in choosing the best option. The goal functions' performance was enhanced by the optimization process's chosen parameters, which proved to be appropriate. QPSO significantly reduces the cost, power losses, voltage variations, and emissions in the modified IEEE 33-bus test system, given the suggested modifications currently in use. Thus, the findings presented provide a strong foundation for future research and practical applications in this important field of power system engineering.

Future studies should apply quantum mechanics to more expansive, varied networks and actual smart grids, integrating demand response techniques, energy storage, and sophisticated communication protocols. The goal of this expansion is to improve the approaches' resilience and suitability for intricate, real-world energy systems. Future studies should also examine how cutting-edge analytics methods like deep learning and AI-driven optimization may lower losses, total generation costs, emissions, and enhance energy management models. These techniques enhance PCC power exchange and help grid-connected MG operators make the best choices feasible by extracting intricate patterns from intricate energy data. This study concludes by emphasizing the need for further research and development to enhance the scalability of optimization techniques for easier implementation and improved performance in large-scale IEEE 69- and 70-bus test systems.

CRediT authorship contribution statement

Kayode Ebenezer Ojo: Writing – review & editing, Writing –

original draft, Investigation, Conceptualization. **Akshay Kumar Saha:** Writing – review & editing, Supervision, Investigation, Conceptualization. **Viranjay M. Srivastava:** Supervision.

Declaration of competing interest

The authors declare that they have no known competing financial interests or personal relationships that could have appeared to influence the work reported in this paper.

Data availability

The data is embedded in the article.

References

[1] I.U. Salam, M. Yousif, M. Numan, K. Zeb, M. Billah, Optimizing distributed generation placement and sizing in distribution systems: a multi-objective analysis of power losses, reliability, and operational constraints, Energies. (Basel) 16 (2023) 5907, https://doi.org/10.3390/en16165907.

[2] M.A. Aman, X.C. Ren, W.U.K. Tareen, M.A. Khan, M.R. Anjum, A.M. Hashmi, H. Ali, I. Bari, J. Khan, S. Ahmad, Optimal siting of distributed generation units in power distribution systems considering voltage profile and power losses, Math. Probl. Eng. 2022 (2022) 1–14, https://doi.org/10.1155/2022/5638407.

[3] K.E. Ojo, A.K. Saha, V.M. Srivastava, Review of advances in renewable energy-based microgrid systems: control strategies, emerging trends, and future possibilities, Energies. (Basel) 18 (2025) 3704, https://doi.org/10.3390/en18143704.

[4] A.M. Tudose, D.O. Sidea, I.I. Picioroaga, N. Anton, C. Bulac, Increasing distributed generation hosting capacity based on a sequential optimization approach using an improved salp swarm algorithm, Mathematics 12 (2024) 48, https://doi.org/10.3390/math12010048.

[5] M.H. Khan, A. Ulasyar, A. Khattak, H. Sheh Zad, M. Alsharef, A.A. Alahmadi, N. Ullah, Optimal sizing and allocation of distributed generation in the radial power distribution system using honey badger algorithm, Energies. (Basel) 15 (16) (2022) 5891, https://doi.org/10.3390/en15165891.

[6] D.B. Aeggegn, G.N. Nyakoe, C. Wekesa, A state-of-the-art review on energy management techniques and optimal sizing of DERs in grid-connected multi-microgrids, Cogent. Eng. 11 (2024) 1–20, https://doi.org/10.1080/23311916.2024.2340306.

[7] P.S. Meera, S. Hemamalini, Reliability assessment and enhancement of distribution networks integrated with renewable distributed generators: a review, Sustain. Energy Technol. Assess. 54 (2022) 102812, https://doi.org/10.1016/j.seta.2022.102812.

[8] K.E. Ojo, A.K. Saha, V.M. Srivastava, Microgrids' control strategies and real-time monitoring systems: a comprehensive review, Energies. (Basel) 18 (2025) 3576, https://doi.org/10.3390/en18133576.

[9] A. Sabir, S. Ibrir, A robust control scheme for grid-connected photovoltaic converters with low-voltage ride-through ability without phase-locked loop, ISA Trans. 96 (2020) 287–298, https://doi.org/10.1016/j.isatra.2019.05.027.

[10] R. Sepehrzad, A. Moridi, M.E. Hassanzadeh, A.R. Seifi, Intelligent energy management and multi-objective power distribution control in hybrid micro-grids based on the advanced fuzzy-PSO method, ISA Trans. 112 (2021) 199–213, https://doi.org/10.1016/j.isatra.2020.12.027.

[11] N. Güler, Irmak E. Design, implementation and model predictive based control of a mode-changeable DC/DC converter for hybrid renewable energy systems, ISA Trans. 114 (2021) 485–498, https://doi.org/10.1016/j.isatra.2020.12.023.

[12] U.P. Vemana, B. Lavanya, N. Rajania, N.K.V. Rao, S. Sirisha, R.S.K. Namburi, C. Prasad, J.M. Ramprasad, D.K. Thilaka, Kishore, Genetic algorithm-based optimization for AVR and DG placement in distribution networks, J. Electr. Syst. 20 (11) (2024) 1068–1074.

[13] M. Kashyap, S. Kansal, R. Verma, Sizing and allocation of DGs in a passive distribution network under various loading scenarios, Electr. Power Syst. Res. 209 (2022) 108046, https://doi.org/10.1016/j.epsr.2022.108046.

[14] S.I. Taheri, M. Davoodi, M.H. Ali, A simulated-annealing–quasi-oppositional–teaching–learning-based optimization algorithm for distributed generation allocation, Computation 11 (214) (2023) 214, https://doi.org/10.3390/computation11110214.

[15] Z.M. Yasin, N.A. Salim, H. Mohamad, N.F Ab Aziz, Adaptive network reconfiguration for distributed generation considering load variability using Ant Lion Optimizer, PaperASIA 41 (5B) (2025) 393–401, https://doi.org/10.59953/paperasia.v41i5b.496.

[16] N. Mezhoud, A. Bahri, B. Ayachi, F. Boukhenoufa, L. Bouras, Optimal placement and sizing of renewable distributed generators for power loss reduction in microgrid using swarm intelligence and bio-inspired algorithms, Sci. Eng. Technol. 5 (1) (2025) 1–14, https://doi.org/10.54327/set2025/v5.i1.208.

[17] H. Prasad, K. Subbaramaiah, P. Sujatha, Optimal DG unit placement in distribution networks by multi-objective whale optimization algorithm and its techno-economic analysis, Electr. Power Syst. Res. 214 (2023) 108869, https://doi.org/10.1016/j.epsr.2022.108869.

[18] G. Derakhshan, H. Shahsavari, A. Safari, Co-evolutionary multi-swarm PSO based optimal placement of miscellaneous DGs in a real electricity grids regarding uncertainties, J. Oper. Autom. Power Eng. 10 (2022) 71–79.

[19] A. Ramadan, M. Ebeed, S. Kamel, E.M. Ahmed, Tostado-Véliz M. Optimal allocation of renewable DGs using artificial hummingbird algorithm under uncertainty conditions, Ain Shams Eng. J. 14 (101872) (2023) 101872, https://doi.org/10.1016/j.asej.2022.101872.

[20] W. Haider, S.J. Ul Hassan, A. Mehdi, A. Hussain, G.O.M. Adjayeng, C.H Kim, Voltage profile enhancement and loss minimization using optimal placement and sizing of distributed generation in reconfigured network, Machines 9 (2021) 20, https://doi.org/10.3390/machines9010020.

[21] N.R. Godha, V.N. Bapat, I. Korachagaon, Ant colony optimization technique for integrating renewable DG in distribution system with techno-economic objectives, Evolving Syst 13 (2022) 485–498, https://doi.org/10.1007/s12530-021-09416-y.

[22] S.I. Taheri, M.B.C. Salles, A.B. Nassif, Distributed energy resource placement considering hosting capacity by combining teaching-learning-based and honey-bee-mating optimization algorithms, Appl. Soft. Comput. 113 (2021) 107953, https://doi.org/10.1016/j.asoc.2021.107953.

[23] A. Shaheen, R. El-Sehiemy, S. Kamel, A. Selim, Optimal operational reliability and reconfiguration of electrical distribution network based on jellyfish search algorithm, Energies. (Basel) 15 (2022) 6994, https://doi.org/10.3390/en15196994.

[24] H. Shokouhandeh, M.R. Ghaharpour, H.G. Lamouki, Y.R. Pashakolae, F. Rahmani, M.H. Imani, Optimal estimation of capacity and location of wind, solar and fuel cell sources in distribution systems considering load changes by lightning search algorithm, in: Proc IEEE Texas Power and Energy Conf (TPEC), College Station, TX, USA, 6–7, 2020, pp. 1–6.

[25] D.X. Tittu George, R. Edwin Raj, A. Rajkumar, M. Carolin Mabel, Optimal sizing of solar–wind based hybrid energy system using modified dragonfly algorithm for an institution, Energy Convers. Manage. 283 (116938) (2023) 116938, https://doi.org/10.1016/j.enconman.2023.116938.

[26] A. Shaheen, R. El-Sehiemy, S. Kamel, A. Selim, Reliability improvement-based reconfiguration of distribution networks via social network search algorithm, in: Proc 23rd Int Middle East Power Syst Conf (MEPCON 2022), Cairo, Egypt, 2022, pp. 1–6, https://doi.org/10.1109/MEPCON55441.2022.10021721.

[27] A.B. Alyu, A.O. Salau, B. Khan, J.N. Eneh, Hybrid GWO-PSO based optimal placement and sizing of multiple PV-DG units for power loss reduction and voltage profile improvement, Sci. Rep. 13 (6903) (2023) 1–17, https://doi.org/10.1038/s41598-023-34057-3.

[28] L.F. Grisales-Noreña, B.J. Restrepo-Cuestas, B. Cortés-Caicedo, J. Montano, A. A. Rosales-Muñoz, M. Rivera, Optimal location and sizing of distributed generators and energy storage systems in microgrids: a review, Energies. (Basel) 16 (2023) 106, https://doi.org/10.3390/en16010106.

[29] A.M. Shaheen, A.M. Elsayed, R.A. El-Sehiemy, A.Y. Abdelaziz, Equilibrium optimization algorithm for network reconfiguration and distributed generation allocation in power systems, Appl. Soft. Comput. 98 (2021) 106867, https://doi.org/10.1016/j.asoc.2020.106867.

[30] B.K. Malik, B.K. Sahu, V. Pattanaik, M. Bajaj, S. Panda, V. Blazek, P.K. Rout, L. Prokop, A critical review of distribution system planning: optimal placement and sizing of distributed generation and energy storage devices in microgrids, Energy Strategy Rev. 62 (2025) 101947, https://doi.org/10.1016/j.esr.2025.101947.

[31] P.D. Huy, V.K. Ramachandaramurthy, J.Y. Yong, K.M. Tan, J.B. Ekanayake, Optimal placement, sizing and power factor of distributed generation: a comprehensive study spanning from the planning stage to the operation stage, Energy 195 (117011) (2020) 117011, https://doi.org/10.1016/j.energy.2020.117011.

[32] C.A.W. Ngouleu, Y.W. Koholé, F.C.V. Fohagui, G. Tchuen, Techno-economic analysis and optimal sizing of a battery-based and hydrogen-based standalone photovoltaic/wind hybrid system for rural electrification in Cameroon based on meta-heuristic techniques, Energy Convers. Manage. 280 (2023) 116794, https://doi.org/10.1016/j.enconman.2023.116794.

[33] F.S. Mahmoud, A.M. Abdelhamid, A. Al Sumaiti, A.-.H.M. El-Sayed, A.A.Z Diab, Sizing and design of a PV–wind–fuel cell storage system integrated into a grid considering the uncertainty of load demand using the marine predator's algorithm, Mathematics 10 (2022) 3708, https://doi.org/10.3390/math10193708.

[34] M. El Marghichi, A. Loulijat, S. Dangoury, H. Chojaa, A.Y. Abdelaziz, M.A. Mossa, J. Hong, S.Z.W Geem, Enhancing battery capacity estimation accuracy using the Bald Eagle Search Algorithm, Energy Rep. 10 (2023) 2710–2724, https://doi.org/10.1016/j.egyr.2023.09.082.

[35] K.E. Ojo, A.K. Saha, V.M. Srivastava, A critical review of advanced protection devices in AC microgrid, IEEe Access. 13 (2025) 203931–203971, https://doi.org/10.1109/ACCESS.2025.3638604.

[36] A. Anvari-Moghaddam, A.R. Seifi, T. Niknam, M.R Alizadeh Pahlavani, Multi-objective operation management of a renewable micro-grid with back-up micro-turbine/fuel cell/battery hybrid power source, Energy 36 (11) (2011) 6490–6507, https://doi.org/10.1016/j.energy.2011.09.017.

[37] A. Gautam, R. Shukla, K. Kishore, P. Jain, R.K. Porwal, N. Nallarasan, Analyses of Indian power system frequency, in: Proc. 2020 IEEE Int. Conf. Power Syst. Technol. (POWERCON), Bangalore, India, 2020, pp. 1–6, https://doi.org/10.1109/POWERCON48463.2020.9230532.

[38] J.A.J. Shirley, R.P. Pooja, M.J.B. Reddy, Metaheuristic algorithm-based energy management system for electric vehicle charging station, IEEe Access. 12 (2024) 116354–116367, https://doi.org/10.1109/ACCESS.2024.3446032.

[39] A. Rathore, N.P. Patidar, Optimal sizing and allocation of renewable based distribution generation with gravity energy storage considering stochastic nature

using particle swarm optimization in radial distribution network, J. Energy Storage 35 (2021) 102282, https://doi.org/10.1016/j.est.2021.102282.
[40] K. Paul, B. Jyothi, R.S. Kumar, A.R. Singh, M. Bajaj, B.H. Kumar, I. Zaitsev, Optimizing sustainable energy management in grid-connected microgrids using quantum particle swarm optimization for cost and emission reduction, Sci. Rep. 15 (2025) 5843, https://doi.org/10.1038/s41598-025-90040-0.
[41] A.G. Gad, Particle swarm optimization algorithm and its applications: a systematic review, Arch. Comput. Methods Eng. 29 (2022) 2531–2561, https://doi.org/10.1007/s11831-021-09694-4.
[42] S.U. Umar, T.A. Rashid, A.M. Ahmed, B.A. Hassan, M.R. Baker, Modified bat algorithm: a newly proposed approach for solving complex and real-world problems, Soft. comput. 28 (2024) 7983–7998, https://doi.org/10.1007/s00500-024-09761-5.
[43] S.A. Al-Asadi, S.O Al-Mamory, An improved BAT algorithm using density-based clustering, Inteligencia Artif 26 (2023) 102–123, https://doi.org/10.4114/intartif.vol26iss72pp102-123.
[44] J. Kennedy, R. Eberhart, Particle swarm optimization, in: Proc. ICNN'95—Int. Conf. Neural Networks, Perth, WA, Australia, 27 November–1 December 1995, New York, NY, USA 4, IEEE, 1995, pp. 1942–1948.
[45] K. Tang, C. Meng, Particle swarm optimization algorithm using velocity pausing and adaptive strategy, Symmetry. (Basel) 16 (2024) 661, https://doi.org/10.3390/sym16060661.
[46] J. Sun, B. Feng, W. Xu, Particle swarm optimization with particles having quantum behavior, in: Proc. 2004 Congress on Evolutionary Computation (CEC2004), Portland, OR, USA, 2004, pp. 325–331, https://doi.org/10.1109/CEC.2004.1330875.
[47] N.-R. Zhou, S.-H. Xia, Y. Ma, Y. Zhang, Quantum particle swarm optimization algorithm with the truncated mean stabilization strategy, J. Algorithms Comput. Technol. 21 (2022) 1–23, https://doi.org/10.1007/s11128-021-03380-x.
[48] K.E. Ojo, A.K. Saha, V.M. Srivastava, A sustainable optimization framework for demand-side energy scheduling in grid-connected microgrid management system, Sustainability. 18 (6) (2026) 2763, https://doi.org/10.3390/su18062763.
[49] M.H. Gadallah, A.A Mohamed Ahmed, A comprehensive review on the classification of multi-objective optimization techniques, Open J. Optim. 14 (2025) 181–228, https://doi.org/10.4236/ojop.2025.144010.
[50] M. Esmaeili, M. Sedighizadeh, M. Esmaili, Multi-objective optimal reconfiguration and DG (distributed generation) power allocation in distribution networks using Big Bang–Big Crunch algorithm considering load uncertainty, Energy 103 (2016) 86–99, https://doi.org/10.1016/j.energy.2016.02.152.
[51] H.R.S. Haneef, Z. Rashid, S.A. Haider, Z.A. Arfeen, N. Husain, A. Yahya, M. Amjad, H. Rehman, Stochastic optimal PV placement and command-based power control for voltage and power factor correction using MOPSO algorithm, Ain Shams Eng. J. 15 (2024) 102990, https://doi.org/10.1016/j.asej.2024.102990.
[52] A. Selim, S. Kamel, F. Jurado, Efficient optimization technique for multiple DG allocation in distribution networks, Appl. Soft. Comput. 86 (2020) 105938, https://doi.org/10.1016/j.asoc.2019.105938.
[53] E. Karunarathne, J. Pasupuleti, J. Ekanayake, D. Almeida, Optimal placement and sizing of DGs in distribution networks using MLPSO algorithm, Energies. (Basel) 13 (2020) 6185, https://doi.org/10.3390/en13236185.
[54] O.M. Suwi, J.J. Justo, M.J. Mighanda, Optimal placement of distributed generation units in power distribution networks using advanced particle swarm optimization, Tanz. J. Eng. Technol. 44 (2025) 319–330, https://doi.org/10.52339/tjet.v44i2.1308.